INTERNATIONAL JOURNAL FOR NUMERICAL AND ANALYTICAL METHODS IN GEOMECHANICS, VOL. 22, 97–132 (1998)

THEORETICAL ANALYSIS OF STRAIN RESPONSE ENVELOPES USING INCREMENTALLY NON-LINEAR CONSTITUTIVE EQUATIONS

P. ROYIS AND T. DOANH

Ecole Nationale des Travaux Publics de l'Etat, DGCB URA 1652, 69518 Vaulx-en-Velin Cedex, France

SUMMARY

This paper reviews some incrementally non-linear constitutive equations of interpolation type, and proposes a new approach to illustrate the discrepancies between different interpolation models. This approach uses the strain response envelopes, based on experimental data when restricted to triaxial plane, and the Jacobian of the constitutive equations to examine the loss of uniqueness. A new family of interpolation functions is proposed to meet the three requirements: $\mathscr{C}^1$-continuity of strain response envelope, correct description of experimental data, and respect of the one-to-one property. © 1998 by John Wiley & Sons, Ltd.

Int. J. Numer. Anal. Meth. Geomech., Vol. 22, 97–132 (1998)
(No. of Figures: 15 No. of Tables: 5 No. of Refs: 21)

Key words: constitutive model; rate-independent type; strain response envelope; granular material; uniqueness

1. INTRODUCTION

Over the past 20 years, incrementally non-linear constitutive equations with interpolation functions have been introduced to describe the complex behaviour of geomaterials. The last two international workshops at Grenoble[1] and at Cleveland[2] on constitutive equations have shown the capacity of this rate-type framework to simulate correctly the mechanical responses of materials, including the effects of principal stress rotation, the incrementally non-linearity or the cyclic loading. Darve's octolinear interpolation[3] is the best known of this framework, but many other interpolation functions have been elaborated. Unfortunately, there is no certainty that the newly proposed functions can meet the incrementally non-linearity conditions and the one-to-one property.

The response envelope introduced by Gudehus[4] is a convenient tool to test the validity of any constitutive equations when restricted to two dimensions as in the triaxial plane. This technique is widely used,[5–8] but the constitutive equations can satisfy the test of the two-dimensional response envelope and fail to meet the three-dimensional incrementally non-linearity. In order to classify the constitutive equations, an adaptation of the strain response envelope for non-axisymmetric stress states is also proposed.[9] Other basic features of soil behaviours are also required as basic guidelines in the development of any constitutive equations,[10] but they are not in the scope of this paper.

*Correspondence to T. Doanh, Ecole Nationale des Travaux Publics de l'Etat, DGCB URA 1652, 69518 Vaulx-en-Velin Cedex, France.

CCC 0363–9061/98/020097–36$17.50

Received May 1996
Revised May 1997

This paper proposes a critical review of different interpolation functions involved in the incrementally non-linear constitutive equations. The strain response envelopes based on observed experimental results are used to evaluate these interpolation functions. A generalization of this technique, using a cartographical representation, is proposed to check the one-to-one property three-dimensionally.

The last objective of this paper is to present a new family of interpolation functions that can meet the three following requirements: $\mathscr{C}^1$-continuity of strain response envelope, correct description of the experimental data, and respect of the one-to-one property.

2. EXPERIMENTAL OBSERVATIONS

Three initial stress states of stress level along the conventional drained axisymmetric triaxial test are used. They are designated as isotropic, intermediate and close to failure. In each series of constant stress ratio, the stress paths are chosen to cover the whole triaxial plane and to obtain accurately the elliptical response generated by the strain increments. The size of the stress increment, 10 kPa, is small enough to represent the incremental behaviour of the Hostun dense sand, and large enough to measure the material response. Table I gives the initial stress states of the stress-probe tests.

The axial and radial principal stresses are denoted by σ_1 and σ_3, respectively, whereas the failure ratio R is defined from the deviatoric stress $\sigma_1 - \sigma_3$ as follows

$$R = \frac{(\sigma_1 - \sigma_3)_{\text{initial}}}{(\sigma_1 - \sigma_3)_{\text{failure}}} \tag{1}$$

Figure 1 shows the stress–strain relationship and the volumetric behaviour of a reference test of Hostun dense sand which is a conventional compression triaxial test under a confining pressure of 100 kPa. All tests have the same density 1·56. The slope of the failure in the q–p' plane is about 1·7. This reference test has a maximum deviator stress of 400 kPa. This sample contracts slightly at the beginning and a dilatancy behaviour is observed at large strains.

The hollow circles indicate the initial position of the three series on the reference test. The first tests series studied the incremental behaviour at the isotropic stress state with 10 probe tests. The second series examined the incremental behaviour at an intermediate stress state where the ratio R is only 0·25. This intermediate stress state is located in the contractive zone, and the initial axial strain is relatively small, about 0·5 per cent. The initial stress state of the last tests series is situated near the failure envelope in the dilative zone, since the failure ratio is greater, about 0·75. The initial axial strain at the beginning of the probe test is much larger, about 3·0 per cent. For the rest of this paper, the origin of the strains (axial and radial) is taken at the beginning of the probe test.

Table I. Initial stress states of probe tests

State	σ_1 (kPa)	σ_3 (kPa)	Stress ratio R
A (Isotropic)	100	100	0·00
B (Intermediate)	200	100	0·25
C (Near failure)	400	100	0·75

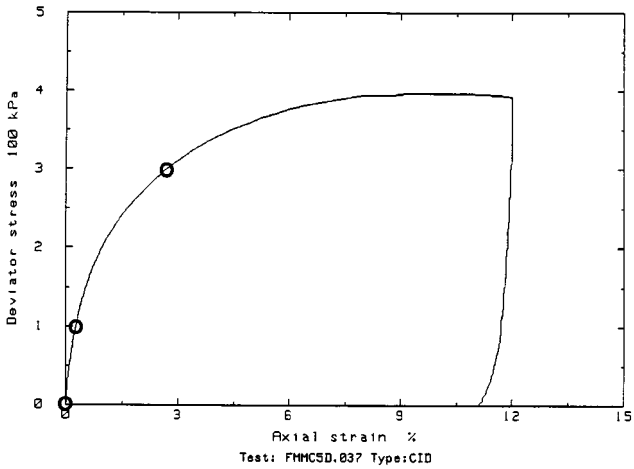

Figure 1a. Reference test on a dense Hostun sample, Stress–strain behaviour

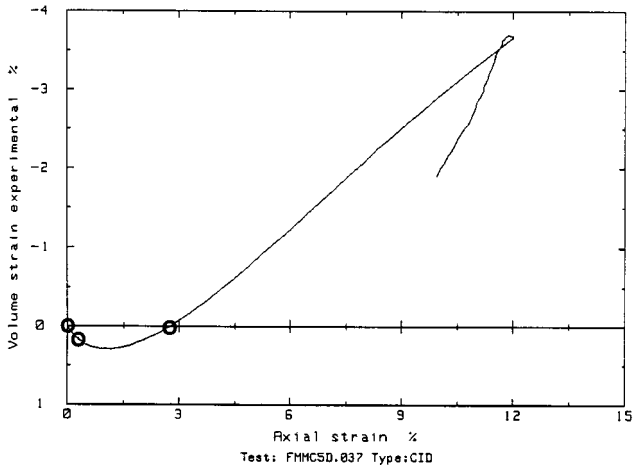

Figure 1b. Reference test on a dense Hostun sample, Volumetric behaviour

In a typical stress-probe test, an isotropically consolidated sample was sheared in drained condition to the desired initial stress state. Then, an incremental stress-probe test was conducted along a constant stress increment direction. Figure 2 represents the direction $\alpha_{\delta\sigma}$ of the stress increments of all probe tests in the axisymmetric triaxial plane. The stress envelope is indicated by a dotted circle. Table II gives the direction $\alpha_{\delta\varepsilon}$ (in the same plane) and the amplitude of the strain increment associated with the direction $\alpha_{\delta\sigma}$ of the stress increment of each probe test. The direction $\alpha_{\delta\sigma}$ is the angle between the positive radial stress axis $\sqrt{2}\sigma_3$ and the stress-probe increment, whereas $\alpha_{\delta\varepsilon}$ is the angle between the positive radial strain axis $\sqrt{2}\varepsilon_3$ and the strain response increment. The values of these directions are in degrees. Note that each probe test was conducted on a new virgin sample.

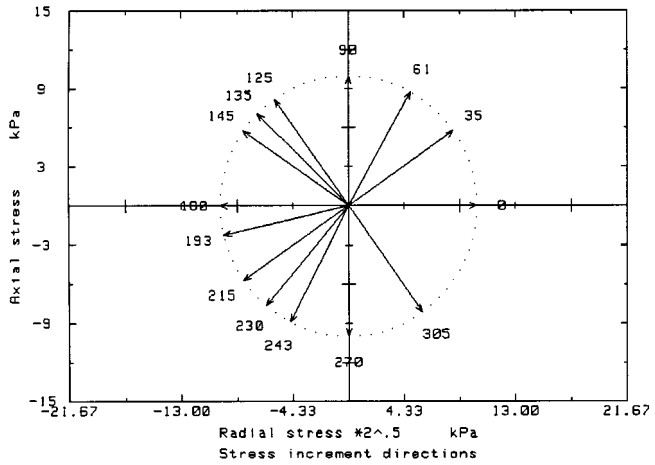

Figure 2. Direction of stress probe tests

Table II. Strain increment responses of probe tests

	100 kPa		200 kPa		400 kPa	
$\alpha_{\delta\sigma}$	$\alpha_{\delta\varepsilon}$	per cent	$\alpha_{\delta\varepsilon}$	per cent	$\alpha_{\delta\varepsilon}$	per cent
0	− 47	0·018	− 15	0·0045	83	0·0126
35	− 10	0·0068	73	0·0091	123	0·0126
61			107	0·0273		
90	100	0·015	112	0·050	129	0·316
125	122	0·036	115	0·0618	130	0·462
135			124	0·0618		
145			130	0·0455		
180	132	0·034	135	0·0273	132	0·633
193	160	0·011				
215	− 165	0·0068	142	0·0182	134	0·433
230	− 81	0·015	155	0·009		
243			− 90	0·0045		
270	− 65	0·032	− 75	0·0068	− 72	0·0063
305	− 56	0·025	− 32	0·0045	− 30	0·0063

Figure 3 shows the results of 10 probe tests starting from the isotropic stress state. The corresponding stain responses form an ellipse in which the initial strain is the centre of the response envelope. The stress-probe tests rotate successively in the counterclockwise direction on the stress envelope, the strain responses also rotate in the same direction on the response envelope. The values of the directions of the stress increments are also superimposed on the strain response envelope. Theoretically, only four particular directions are enough to identify the constitutive coefficients of the tangent matrices, but practically 10 probe tests are needed to identify correctly the shape of the strain envelope which is nearly symmetric with respect to the origin of the axis.

The strain envelope of the intermediate stress state is determined with 13 probe tests, Figure 4, and the last stress state with only eight tests, Figure 5. Globally, the shapes of the response

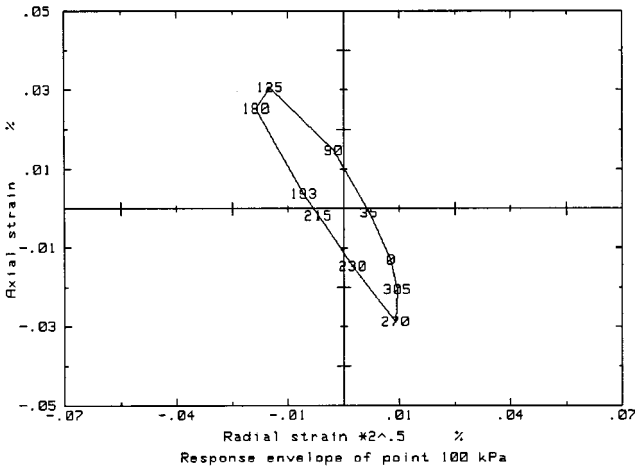

Figure 3. Strain response envelope of point 100, 100 kPa

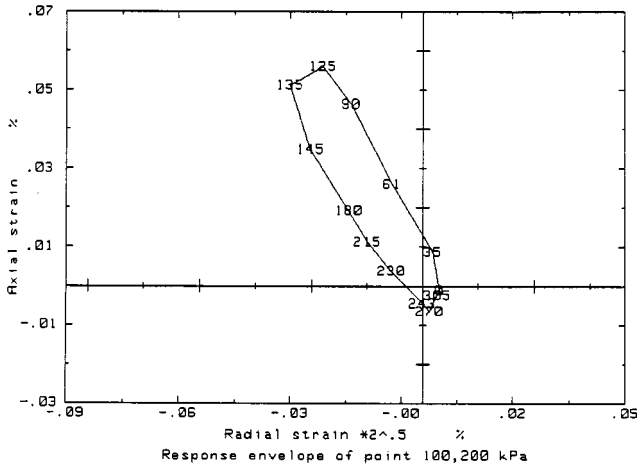

Figure 4. Strain response envelope of point 200, 100 kPa

envelopes are similar but more elongated and shifted away from the original axes, indicating the irreversibility of the material. The response envelopes tend to be stretched in the directions located between 125° and that of the radial extension test. Furthermore, as the initial stress ratio increases, the response envelope seems to degenerate into a very flat envelope.

3. DESCRIPTION OF THE CONSTITUTIVE MODELS

3.1. General considerations

In this section we are interested in a particular class of incrementally non-linear constitutive models. The use of such models to describe the non-linear behaviour of geomaterials, such as soils

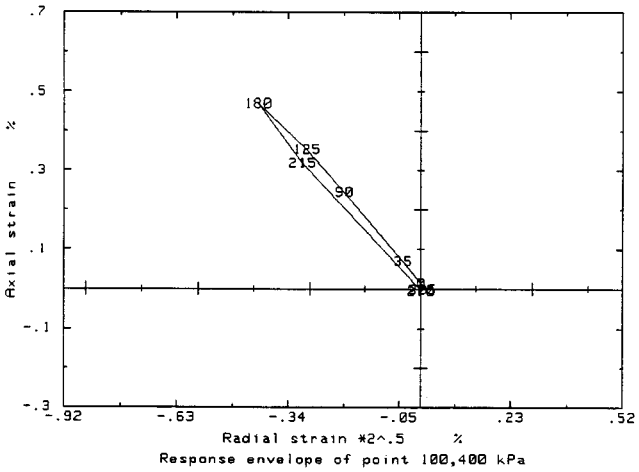

Figure 5. Strain response envelope of point 400, 100 kPa

or concrete, is well established and many rheologicals models have been issued from this formalism.[11,12]

Let us consider materially simple media without any viscous properties, for which the influence of the temperature on the mechanical behaviour may be ignored. We assume the existence of an initial state of the medium with intact stress and strain history, with respect to which the constitutive equations are isotropic.

For that class of media the general form of incremental constitutive models considered in this paper consists of a non-linear function involving the strain rate tensor $\mathbf{D}$ and the objective Jaumann derivative $\hat{\boldsymbol{\sigma}}$ of the Cauchy stress tensor $\boldsymbol{\sigma}$

$$\mathbf{D} = \mathbf{F}(\hat{\boldsymbol{\sigma}}) \tag{2}$$

where the tensorial function $\mathbf{F}$ depends, at each material point $\mathbf{x}$ and at every time t, on the whole previous stress and strain history at the point considered. Note that the inverse approach which consists in expressing $\hat{\boldsymbol{\sigma}}$ as a function of $\mathbf{D}$ and from which other incrementally non-linear constitutive models are issued,[8,13] or the recent hypoplasticity approach,[14–16] are not within the scope of this paper. Let us recall that $\hat{\boldsymbol{\sigma}}$ is defined by

$$\hat{\boldsymbol{\sigma}} = \dot{\boldsymbol{\sigma}} + \boldsymbol{\sigma}\cdot\mathbf{W} - \mathbf{W}\cdot\boldsymbol{\sigma} \tag{3}$$

where $\dot{\boldsymbol{\sigma}}$ is the material derivative of $\boldsymbol{\sigma}$ and $\mathbf{W}$ is the spin tensor, that is to say, it is the skew-symmetric part of the gradient $\mathbf{G} = \mathrm{grad}_{\mathbf{x}}(\mathbf{v})$ of the velocity field $\mathbf{v}$ at point $\mathbf{x}$, of which $\mathbf{D}$ is the symmetric part.

Let $\mathscr{T}_2^s(\mathbb{R}^3)$ be the six-dimensional vector space of second-order symmetric tensors on the real three-dimensional orthonormal vector space $\mathbb{R}^3$, and let $\mathbb{R}^6$ be the real six-dimensional orthonormal vector space. We shall associate every tensor $\mathbf{T} \in \mathscr{T}_2^s(\mathbb{R}^3)$ with a vector $\mathbf{T} \in \mathbb{R}^6$, the

components of which are determined as follows:

$$\mathbf{T} = \begin{bmatrix} T_{11} & T_{12} & T_{13} \\ T_{12} & T_{22} & T_{23} \\ T_{13} & T_{23} & T_{33} \end{bmatrix} \Leftrightarrow \mathbf{T} = \begin{bmatrix} T_1 \\ T_2 \\ T_3 \\ T_4 \\ T_5 \\ T_6 \end{bmatrix} \text{ with } \begin{cases} T_1 = T_{11} \\ T_2 = T_{22} \\ T_3 = T_{33} \\ T_4 = \sqrt{2}T_{23} \\ T_5 = \sqrt{2}T_{13} \\ T_6 = \sqrt{2}\mathrm{T}_{12} \end{cases} \tag{4}$$

This relation, which defines an isometric isomorphism Φ between $\mathscr{T}_2^s(\mathbb{R}^3)$ and $\mathbb{R}^6$, verifies the following property:

Property 1. Let us consider an orthonormal transformation of $\mathbb{R}^3$, *defined by the orthogonal matrix* $\mathbf{P}$. *We have then, for the vectors of* $\mathbb{R}^6$ *associated by* Φ *to the tensors of* $\mathscr{T}_2^s(\mathbb{R}^3)$, *an orthonormal transformation of* $\mathbb{R}^6$ *defined by an orthogonal matrix* $\mathbf{Q}$, *the components* Q_{ij} *of which are functions of the components* P_{ij} *of* $\mathbf{P}$.

The proof of this property can be found in reference.[17] So, bearing in mind expression (4), relation (2) becomes

$$\mathbf{D} = \mathbf{F}(\hat{\boldsymbol{\sigma}}) \tag{5}$$

Let us note that the functions $\mathbf{F}$ are defined on the whole space $\mathbb{R}^6$, and not on a proper subset of it, which involves the impossibility of describing softening as well as ideal plastic behaviour, the last one being only described in an asymptotical way by the constitutive models considered.

Equation (5) describes the behaviour of materials without any viscous property. This implies[11] that $\mathbf{F}$ is positively homogeneous of degree one in $\hat{\boldsymbol{\sigma}}$, that is to say homogeneous in a sense restricted to the positive values of the multiplicative parameter λ

$$\forall \lambda \geqslant 0, \quad \forall \hat{\boldsymbol{\sigma}} \in \mathbb{R}^6 : \mathbf{F}(\lambda \hat{\boldsymbol{\sigma}}) = \lambda \mathbf{F}(\hat{\boldsymbol{\sigma}}) \tag{6}$$

Therefore, $\mathbf{F}$ obeys Euler's identity for homogeneous functions. Let then $\mathbf{J}$ denote the gradient tensor of $\mathbf{F}$, the components of which are defined by

$$\forall (i, j) \in \{1, 2, 3, 4, 5, 6\}^2 : J_{ij} = \frac{\partial F_i}{\partial \hat{\sigma}_j} \tag{7}$$

So we obtain

$$\mathbf{D} = \mathbf{J} \cdot \hat{\boldsymbol{\sigma}} \tag{8}$$

The second-order tensor $\mathbf{J}$ is then homogeneous of degree 0 in $\hat{\boldsymbol{\sigma}}$, in a sense restricted to the strictly positive values of the multiplicative parameter λ

$$\forall \lambda > 0, \quad \forall \hat{\boldsymbol{\sigma}} \in \mathbb{R}^{6*} : \mathbf{J}(\lambda \hat{\boldsymbol{\sigma}}) = \mathbf{J}(\hat{\boldsymbol{\sigma}}) \tag{9}$$

This means that $\mathbf{J}$ only depends, in addition to the whole previous stress and strain history at the material point considered, on the direction $\mathbf{d}$ of $\hat{\boldsymbol{\sigma}}$

$$\forall \hat{\boldsymbol{\sigma}} \in \mathbb{R}^{6*} : \mathbf{J}(\hat{\boldsymbol{\sigma}}) = \mathbf{J}(\mathbf{d}) \quad \text{with } \mathbf{d} = \frac{\hat{\boldsymbol{\sigma}}}{\| \hat{\boldsymbol{\sigma}} \|} \tag{10}$$

where $\| \hat{\boldsymbol{\sigma}} \| = \sqrt{\hat{\sigma}_i \hat{\sigma}_i}$ is the Euclidian norm of $\hat{\boldsymbol{\sigma}}$.

Finally, we shall assume the existence, at each material point $\mathbf{x}$ and at every time t, of an orthonormal frame of $\mathbb{R}^3$ with respect to which the constitutive equations are orthotropic. In other words, the group of material symmetry at the time and point considered is generated by the three symmetries associated to each of the three orthogonal planes defined by this frame, which is called the orthotropy frame at point $\mathbf{x}$ and at time t. Note that this assumption turns into a theorem[18] if the set of the tensor fields describing the material history of the medium is reduced to the only Cauchy stress tensor $\boldsymbol{\sigma}$.

The first stage in the general formulation of constitutive equations (5) (which consist of a non-linear map of $\mathbb{R}^6$ onto $\mathbb{R}^6$ depending on the previous stress and strain history) is their restriction to a particular class of stress paths called 'generalized triaxial paths', which can be obtained with a triaxial apparatus. On these paths the principal axes of the tensors $\mathbf{D}$ and $\hat{\boldsymbol{\sigma}}$ are fixed and identical to the orthotropy axes of the material, at each material point and at every time. So we associate these tensors, represented by diagonal matrices in the orthotropy frame of the material, with the vectors of $\mathbb{R}^3$ obtained by keeping only the first three components of the vectors of $\mathbb{R}^6$ defined by the correspondence (4). For such paths the expression (5) is then reduced to a map of $\mathbb{R}^3$ onto $\mathbb{R}^3$ that gives the expression of the constitutive model restricted to these particular paths. For a given history this restricted model is then obtained from the responses $\mathbf{D}$ to the six particular solicitations $\hat{\boldsymbol{\sigma}}$ defined by $\hat{\sigma}_j = \pm\, \delta_{ij}, j \in \{1, 2, 3\}$, where i describes the set $\{1, 2, 3\}$. These six responses allow to define the following matrices:

$$\mathbf{R}^+ = \begin{bmatrix} \dfrac{1}{E_1^+} & \dfrac{-\nu_{12}^+}{E_2^+} & \dfrac{-\nu_{13}^+}{E_3^+} \\ \dfrac{-\nu_{21}^+}{E_1^+} & \dfrac{1}{E_2^+} & \dfrac{-\nu_{23}^+}{E_3^+} \\ \dfrac{-\nu_{31}^+}{E_1^+} & \dfrac{-\nu_{32}^+}{E_2^+} & \dfrac{1}{E_3^+} \end{bmatrix}, \qquad \mathbf{R}^- = -\begin{bmatrix} \dfrac{1}{E_1^-} & \dfrac{-\nu_{12}^-}{E_2^-} & \dfrac{-\nu_{13}^-}{E_3^-} \\ \dfrac{-\nu_{21}^-}{E_1^-} & \dfrac{1}{E_2^-} & \dfrac{-\nu_{23}^-}{E_3^-} \\ \dfrac{-\nu_{31}^-}{E_1^-} & \dfrac{-\nu_{32}^-}{E_2^-} & \dfrac{1}{E_3^-} \end{bmatrix} \tag{11}$$

which are called 'tangent constitutive matrices'. The column i of $\mathbf{R}^+$ (resp. $\mathbf{R}^-$), $i \in \{1, 2, 3\}$, constitutes the response to the solicitation defined by $\hat{\sigma}_j = +\, \delta_{ij}$, (resp. $\hat{\sigma}_j = -\, \delta_{ij}$), $j \in \{1, 2, 3\}$. The various quantities $E_i^{\pm}$, $i \in \{1, 2, 3\}$, and $\nu_{ij}^{\pm}$, $(\mathrm{i}, \mathrm{j}) \in \{1, 2, 3\}^2$, defining these two matrices are often called 'tangent Young moduli' and 'tangent Poisson ratios', respectively. They are strictly positive for all the models we shall consider in the following. For a given solicitation path the determination of these tangent matrices constitutes the simulation of the behaviour memory and is the hearth of the constitutive model. Its complexity reflects that of the physical phenomenon that is describes. The response $\mathbf{D}$ to any solicitation $\hat{\boldsymbol{\sigma}} \in \mathbb{R}^3$ is then obtained by interpolation from the six previous responses, which achieves the construction of the restricted model. So the stage relating to interpolation, which constitutes the main subject of Section 3.2, is dissociated from that of building the tangent constitutive matrices.

The constitutive model restricted to the previous triaxial paths must then be generalized to any path. This last stage, which requires some assumptions, is not within the scope of this paper. For details, the reader can refer to Chambon[18] or to Royis.[17]

3.2. The restricted models

Now we are interested in the interpolations relating to ten incremental constitutive models, we shall denote by the symbols L1 to L10 in the following. L1 is the octolinear Darve model[3] and L2

the non-linear one.[11] L3 and L4 denote, respectively, the first and second non-linear models of Chambon,[18] which are called A2 and A2bis by their author, whereas L5 and L6 correspond to those of Di Benedetto.[19] L7 and L8 are the non-linear models of Robinet *et al.*[1] and Doanh *et al.*[2] respectively. Finally we denote by L9 and L10 the two non-linear models issued from a family developed by Royis.[20]

In the following, we shall only consider the restriction of the previous ten models to the set of generalized triaxial paths described in Section 3.1. On such paths the principal axes of the tensors $\mathbf{D}$ and $\hat{\boldsymbol{\sigma}}$ are fixed and identical with the orthotropy axes of the material, at each material point and at every time. These tensors are then represented by diagonal matrices in the orthotropy frame

$$\mathbf{D} = \begin{bmatrix} D_1 & 0 & 0 \\ 0 & D_2 & 0 \\ 0 & 0 & D_3 \end{bmatrix}, \qquad \hat{\boldsymbol{\sigma}} = \begin{bmatrix} \hat{\sigma}_1 & 0 & 0 \\ 0 & \hat{\sigma}_2 & 0 \\ 0 & 0 & \hat{\sigma}_3 \end{bmatrix} \tag{12}$$

and we shall associate these diagonal matrices with the following vectors of $\mathbb{R}^3$:

$$\mathbf{D} = \begin{bmatrix} D_1 \\ D_2 \\ D_3 \end{bmatrix}, \qquad \hat{\boldsymbol{\sigma}} = \begin{bmatrix} \hat{\sigma}_1 \\ \hat{\sigma}_2 \\ \hat{\sigma}_3 \end{bmatrix} \tag{13}$$

Relations (5) relating to the models L1, L2, L3, L4, L7, L8, L9 and L10 restricted to the class of generalized triaxial paths can then be written, with respect to the orthotropy axes as

$$\mathbf{D} = \| \hat{\boldsymbol{\sigma}} \| \, [\mathbf{R}^+ \cdot \boldsymbol{\psi}^+(\mathbf{d}) + \mathbf{R}^- \cdot \boldsymbol{\psi}^-(\mathbf{d}) + \mathbf{R}^0 \cdot \boldsymbol{\psi}^0(\mathbf{d})] \tag{14}$$

The tangent constitutive matrices $\mathbf{R}^+$ and $\mathbf{R}^-$ are defined by relations (11), and the direction $\mathbf{d}$ of $\hat{\boldsymbol{\sigma}}$ by relation (10). The matrices $\mathbf{R}^0$, the expression of which derives from those of $\mathbf{R}^+$ and $\mathbf{R}^-$, appears only in models L9 and L10, and more generally in all those of the family of non-linear models developed by Royis. By completing the definition of the interpolation, they contribute to avoid the losses of one-to-one properties of the constitutive equations.[20] Their expressions are given, for models L9 and L10, by the following relations (15) and (16), respectively:

$$\begin{cases} \forall (i,j) \in \{1,2,3\}^2 \text{ and without any summation on } i \text{ and } j \\ R^0_{ij} = R^+_{ij} - R^-_{ij} - \varepsilon \sqrt{(R^+_{ij})^2 + (R^-_{ij})^2 + R^+_{ij} R^-_{ij}} \\ \text{with } \varepsilon = +1 \text{ if } R^+_{ij} > 0 \text{ and } \varepsilon = -1 \text{ if } R^+_{ij} < 0 \end{cases} \tag{15}$$

$$\begin{cases} \forall (i,j) \in \{1,2,3\}^2 \text{ and without any summation on } i \text{ and } j \\ R^0_{ij} = 2 \, \dfrac{R^+_{ij} R^-_{ij}}{R^-_{ij} - R^+_{ij}} \end{cases} \tag{16}$$

The vectors $\boldsymbol{\psi}^+$, $\boldsymbol{\psi}^-$ and $\boldsymbol{\psi}^0$, the last one appearing only in models L9 and L10, are the directional interpolation vectors of the eight considered restricted models. Their form, which is

identical except for L4, is as follows:

$$\boldsymbol{\psi}^+(\mathbf{d}) = \begin{bmatrix} \varphi^+(d_1) \\ \varphi^+(d_2) \\ \varphi^+(d_3) \end{bmatrix}, \qquad \boldsymbol{\psi}^-(\mathbf{d}) = \begin{bmatrix} \varphi^-(d_1) \\ \varphi^-(d_2) \\ \varphi^-(d_3) \end{bmatrix}, \qquad \boldsymbol{\psi}^0(\mathbf{d}) = \begin{bmatrix} \varphi^0(d_1) \\ \varphi^0(d_2) \\ \varphi^0(d_3) \end{bmatrix} \tag{17}$$

Then the seven considered restricted models differ only in their interpolation functions $\varphi^+(d)$, $\varphi^-(d)$ and $\varphi^0(d)$, $d \in [-1, 1]$, this last one occurring only in L9 and L10. These functions are shown in Table III.

By combining relations (14) and (17) we can observe that the evaluation of the components D_i of $\mathbf{D}$, $i \in \{1, 2, 3\}$, involves the functions r_{ij}, $(i, j) \in \{1, 2, 3\}^2$, defined by $r_{ij}(d_j) = R_{ij}^+ \varphi^+(d_j) + R_{ij}^- \varphi^-(d_j) + R_{ij}^0 \varphi^0(d_j)$, with $d_j \in [-1, 1]$ and without any summation on j. A new study of these functions will be carried out in Section 5.

As to the interpolation vectors $\boldsymbol{\psi}^+$ and $\boldsymbol{\psi}^-$ relating to the restricted model L4, they are expressed by the following relations, in which the interpolation functions φ^+ and φ^- are those of model L3:

$$\begin{cases} \boldsymbol{\psi}^+(\mathbf{d}) = \phi(\mathbf{d}) \begin{bmatrix} \dfrac{1}{N_1^+}\varphi^+(d_1) \\ \dfrac{1}{N_2^+}\varphi^+(d_2) \\ \dfrac{1}{N_3^+}\varphi^+(d_3) \end{bmatrix}, \qquad \boldsymbol{\psi}^-(\mathbf{d}) = \phi(\mathbf{d}) \begin{bmatrix} \dfrac{1}{N_1^-}\varphi^-(d_1) \\ \dfrac{1}{N_2^-}\varphi^-(d_2) \\ \dfrac{1}{N_3^-}\varphi^-(d_3) \end{bmatrix} \\ \text{with} \begin{cases} \forall i \in \{1, 2, 3\} : N_i^+ = \sqrt{\displaystyle\sum_{k=1}^{k=3} (R_{ki}^+)^2} \; N_i^- = \sqrt{\displaystyle\sum_{k=1}^{k=3} (R_{ki}^-)^2} \\ \phi(\mathbf{d}) = \dfrac{1}{2} \displaystyle\sum_{i=1}^{i=3} (d_i(d_i + |d_i|)N_i^+ + d_i(d_i - |d_i|)N_i^-) \end{cases} \end{cases} \tag{18}$$

Finally, the restricted models L5 and L6 take the form

$$\mathbf{D} = \mathbf{M} \cdot \hat{\boldsymbol{\sigma}} \tag{19}$$

where the matrices $\mathbf{M}$ are given by the following expressions:

$$\begin{cases} \forall (i, j) \in \{1, 2, 3\}^2 \quad \text{and without any summation on } i \text{ and } j \\ \text{L5:} \begin{cases} M_{ij} = 2 \dfrac{R_{ij}^+ R_{ij}^-}{R_{ij}^- - R_{ij}^+ + d_j(R_{ij}^- + R_{ij}^+)} \end{cases} \\ \text{L6:} \begin{cases} M_{ij} = -\dfrac{v_{ij}^+ + v_{ij}^- + d_j(v_{ij}^+ - v_{ij}^-)}{E_j^+ + E_j^- + d_j(E_j^+ - E_j^-)} \\ \text{with } v_{ii}^+ = v_{ii}^- = -1 \quad \forall i \in \{1, 2, 3\} \end{cases} \end{cases} \tag{20}$$

Table III. The several interpolation functions

	$\varphi^+(d)$	$\varphi^-(d)$	$\varphi^0(d)$
L1: Darve's octolinear	$\dfrac{\lvert d\rvert + d}{2}$	$\dfrac{\lvert d\rvert - d}{2}$	0
L2: Darve's non-linear	$\dfrac{d^2 + d}{2}$	$\dfrac{d^2 - d}{2}$	0
L3: Chambon's non-linear	$\dfrac{\lvert d\rvert^3 + d}{2}$	$\dfrac{\lvert d\rvert^3 - d}{2}$	0
L7: Robinet	$d - \dfrac{d}{\Pi}\arccos d$	$-\dfrac{d}{\Pi}\arccos d$	0
L8: Doanh	$\dfrac{d(1+d)^2}{4}$	$\dfrac{-d(1-d)^2}{4}$	0
L9 and L10: Royis	$d\left(\dfrac{\lvert d\rvert + d}{2}\right)$	$-d\left(\dfrac{\lvert d\rvert - d}{2}\right)$	$d(1-\lvert d\rvert)$

In order to study the one-to-one properties of the ten previous restricted models in Section 4.3, we shall now focus on their gradient tensor **J**, the components of which are defined by the relations (7), with $(i,j) \in \{1,2,3\}^2$.

3.3. *The gradient tensors of the restricted models*

The gradient tensors **J** of the restricted models L5 and L6 described in Section 3.2, the components of which are defined, for any $\hat{\boldsymbol{\sigma}} \neq \mathbf{0}$, by the relations (7) with $(i,j) \in \{1,2,3\}^2$, are as follows:

$$\begin{cases} \forall (i,j) \in \{1,2,3\}^2 \\ \text{L5:} \begin{cases} J_{ij} = M_{ij} + 2 \displaystyle\sum_{k=1}^{k=3} \frac{d_k(d_k d_j - \delta_{kj}) R_{ik}^+ R_{ik}^- (R_{ik}^- + R_{ik}^+)}{(R_{ik}^- - R_{ik}^+ + d_k(R_{ik}^- + R_{ik}^+))^2} \\ (\text{without any summation on } i) \end{cases} \\ \text{L6:} \begin{cases} J_{ij} = M_{ij} + 2 \displaystyle\sum_{k=1}^{k=3} \frac{d_k(\delta_{kj} - d_k d_j)(v_{ik}^- E_k^+ - v_{ik}^+ E_k^-)}{(E_k^+ + E_k^- + d_k(E_k^+ - E_k^-))^2} \end{cases} \end{cases} \tag{21}$$

As to the other restricted models L1, L2, L3, L4, L7, L8, L9 and L10, the gradient tensor **J** takes the following general form:

$$\mathbf{J} = \mathbf{R}^+ \cdot \mathbf{J}^+ + \mathbf{R}^- \cdot \mathbf{J}^- + \mathbf{R}^0 \cdot \mathbf{J}^0 \tag{22}$$

in which tensors $\mathbf{J}^+, \mathbf{J}^-$ and $\mathbf{J}^0$, the last one occurring only in L9 and L10, are (except for L4) given by the following relations:

$$\begin{cases} \forall (i,j) \in \{1,2,3\}^2 \text{ and without any summation on } i \\ J_{ij}^+ = d_j \varphi^+(d_i) + (\delta_{ij} - d_i d_j)\varphi^{+\prime}(d_i) \\ J_{ij}^- = d_j \varphi^-(d_i) + (\delta_{ij} - d_i d_j)\varphi^{-\prime}(d_i) \\ J_{ij}^0 = d_j \varphi^0(d_i) + (\delta_{ij} - d_i d_j)\varphi^{0\prime}(d_i) \end{cases} \tag{23}$$

where the functions $\varphi^{+\prime}$, $\varphi^{-\prime}$ and $\varphi^{0\prime}$, the expressions of which are shown in Table IV, are the derivatives of φ^+, φ^- and φ^0, respectively.

Let us note that the components J_{ij}^s of $\mathbf{J}^s$, $s \in \{-, 0, +\}$, satisfy the following relations $J_{ij}^s d_j = \varphi^s(d_i)$, $\forall i \in \{1,2,3\}$. For the generalized triaxial paths considered these relations combined with the expression (22) of $\mathbf{J}$ illustrate the equivalence between expressions (8) and (14) of the strain rate tensor $\mathbf{D}$.

The function 'sgn' that occurs for the restricted model L1 in the definition of $\varphi^{+\prime}$ and $\varphi^{-\prime}$ is worth 1 (resp. -1) if $d > 0$ (resp. $d < 0$). So these two derivatives, which are constant on each of the intervals $[-1, 0[$ and $]0, 1]$, are not defined for $d = 0$. We suggest to take, for $d = 0$, the value at this point of their Fourier series development, which amounts to put $\operatorname{sgn}(0) = 0$.

At last the tensors $\mathbf{J}^+$ and $\mathbf{J}^-$ relating to the restricted model L4 are defined by the following relations:

$$\begin{cases} \forall (i,j) \in \{1,2,3\}^2 \text{ and without any summation on } i \\ \quad J_{ij}^+ = \dfrac{\phi(\mathbf{d})}{N_i^+}\,(d_j \varphi^+(d_i) + (\delta_{ij} - d_i d_j)\varphi^{+\prime}(d_i)) \\ \qquad + \dfrac{\varphi^+(d_i)}{N_i^+} \displaystyle\sum_{k=1}^{k=3} (\delta_{kj} - d_k d_j)((d_k + |d_k|)N_k^+ + (d_k - |d_k|)N_k^-) \\ \quad J_{ij}^- = \dfrac{\phi(\mathbf{d})}{N_i^-}\,(d_j \varphi^-(d_i) + (\delta_{ij} - d_i d_j)\varphi^{-\prime}(d_i)) \\ \qquad + \dfrac{\varphi^-(d_i)}{N_i^-} \displaystyle\sum_{k=1}^{k=3} (\delta_{kj} - d_k d_j)((d_k + |d_k|)N_k^+ + (d_k - |d_k|)N_k^-) \end{cases} \tag{24}$$

where the functions φ^+, φ^-, $\varphi^{+\prime}$ and $\varphi^{-\prime}$ are those of L3, and where the quantities ϕ, N_i^+ and N_i^-, $i \in \{1,2,3\}$, are given by expressions (18).

4. ANALYSIS OF STRAIN RESPONSE ENVELOPE

Now, after determining the values of the constitutive matrices $\mathbf{R}^+$ and $\mathbf{R}^-$, we shall compare the theoretical strain response envelopes of the constitutive models described above with the experimental ones.

Let us note that for all these experimental responses, the strains remain small. So we shall identify, in the following, the tensors $\hat{\boldsymbol{\sigma}}$ and $\mathbf{D}$ with the time derivatives $\dot{\boldsymbol{\sigma}}$ and $\dot{\boldsymbol{\epsilon}}$ of the stress and strain tensor $\boldsymbol{\sigma}$ and $\boldsymbol{\epsilon}$, respectively.

Table IV. The derivatives of the interpolation functions

	$\varphi^{+\prime}(d)$	$\varphi^{-\prime}(d)$	$\varphi^{0\prime}(d)$
L1: Darve's octolinear	$\dfrac{\operatorname{sgn} d+1}{2}$	$\dfrac{\operatorname{sgn} d-1}{2}$	0
L2: Darve's non-linear	$d+\frac{1}{2}$	$d-\frac{1}{2}$	0
L3: Chambon's non-linear	$\dfrac{3d\lvert d\rvert+1}{2}$	$\dfrac{3d\lvert d\rvert-1}{2}$	0
L7: Robinet	$d(\Pi\sqrt{1-d^2})^{-1}$ $-\Pi^{-1}\arccos d+1$	$d(\Pi\sqrt{1-d^2})^{-1}$ $-\Pi^{-1}\arccos d$	0
L8: Doanh	$\dfrac{3d^2+4d+1}{4}$	$\dfrac{-3d^2+4d-1}{4}$	0
L9 and L10: Royis	$d+\lvert d\rvert$	$d-\lvert d\rvert$	$1-2\lvert d\rvert$

4.1. Identification of constitutive matrices

The constitutive equations are completely determined by the matrices of equations (11). And when restricted to the triaxial plane $\sigma_2=\sigma_3$, we have the following equalities between tangent Young moduli and tangent Poisson ratios:

$$\begin{cases} E_2^+ = E_3^+ \\ \nu_{12}^+ = \nu_{13}^+ \\ \nu_{32}^+ = \nu_{23}^+ \\ \nu_{21}^+ = \nu_{31}^+ \end{cases} \quad \text{and} \quad \begin{cases} E_2^- = E_3^- \\ \nu_{12}^- = \nu_{13}^- \\ \nu_{32}^- = \nu_{23}^- \\ \nu_{21}^- = \nu_{31}^- \end{cases} \tag{25}$$

The tangent constitutive 3×3 matrices can be expressed as 2×2 matrices. Dropping the sign $+$ and $-$ on each symbol for the sake of simplicity, we have

$$\begin{pmatrix} \dot\varepsilon_1 \\ \dot\varepsilon_3 \end{pmatrix} = \begin{pmatrix} \dfrac{1}{E_1} & \dfrac{-2\nu_{13}}{E_3} \\ \dfrac{-\nu_{31}}{E_1} & \dfrac{1}{E_3}-\dfrac{\nu_{23}}{E_3} \end{pmatrix} \begin{pmatrix} \dot\sigma_1 \\ \dot\sigma_3 \end{pmatrix} \tag{26}$$

with five parameters E_1, E_3, ν_{31}, ν_{13} and ν_{23} to be identified on the compression (sign $+$) and the extension (sign $-$) side.

For an increment of stress in the direction 1 with $\dot\sigma=(\dot\sigma_1, 0)$ we obtain the first set of equations

$$\begin{pmatrix} \dot\varepsilon_1 \\ \dot\varepsilon_3 \end{pmatrix} = \begin{pmatrix} \dfrac{1}{E_1} & \dfrac{-2\nu_{13}}{E_3} \\ \dfrac{-\nu_{31}}{E_1} & \dfrac{1}{E_3}-\dfrac{\nu_{23}}{E_3} \end{pmatrix} \begin{pmatrix} \dot\sigma_1 \\ 0 \end{pmatrix} = \begin{pmatrix} \dfrac{\dot\sigma_1}{E_1} \\ \dfrac{-\nu_{31}\dot\sigma_1}{E_1} \end{pmatrix} \tag{27}$$

The two coefficients E_1 and v_{31} can be identified by the strain response $\dot{\varepsilon} = (\dot{\varepsilon}_1, \dot{\varepsilon}_3)$

$$\begin{cases} E_1 = \dfrac{\dot{\sigma}_1}{\dot{\varepsilon}_1} \\ v_{31} = -\dfrac{\dot{\varepsilon}_3 E_1}{\dot{\sigma}_1} \end{cases} \tag{28}$$

This means that the coefficients $(E_1^+, v_{31}^+)(E_1^-, v_{31}^-)$ of the constitutive matrices can be identified by an increment of compression stress and an increment of extension stress of direction 1, respectively. The classical triaxial compression $(\dot{\sigma}_1^+, 0)$ and extension $(\dot{\sigma}_1^-, 0)$ increments corresponding to two particular stress increment directions $\alpha_{\dot{\sigma}} = 90^\circ$ and $\alpha_{\dot{\sigma}} = 270^\circ$ give two particular responses $(\dot{\varepsilon}_1^+, \dot{\varepsilon}_3^+)$ in compression and $(\dot{\varepsilon}_1^-, \dot{\varepsilon}_3^-)$ in extension on the strain response envelope

$$\begin{cases} E_1^+ = \dfrac{\dot{\sigma}_1^+}{\dot{\varepsilon}_1^+} \\ v_{31}^+ = -\dfrac{\dot{\varepsilon}_3^+ E_1^+}{\dot{\sigma}_1^+} \end{cases} \quad \text{and} \quad \begin{cases} E_1^- = \dfrac{\dot{\sigma}_1^-}{\dot{\varepsilon}_1^-} \\ v_{31}^- = -\dfrac{\dot{\varepsilon}_3^- E_1^-}{\dot{\sigma}_1^-} \end{cases} \tag{29}$$

For an increment of stress in the direction 3 with $\dot{\sigma} = (0, \dot{\sigma}_3)$ we obtain the second set of equations

$$\begin{pmatrix} \dot{\varepsilon}_1 \\ \dot{\varepsilon}_3 \end{pmatrix} = \begin{pmatrix} \dfrac{1}{E_1} & \dfrac{-2v_{13}}{E_3} \\ \dfrac{-v_{31}}{E_1} & \dfrac{1}{E_3} - \dfrac{v_{23}}{E_3} \end{pmatrix} \quad \begin{pmatrix} 0 \\ \dot{\sigma}_3 \end{pmatrix} = \begin{pmatrix} \dfrac{-2v_{13}\dot{\sigma}_3}{E_3} \\ \left(\dfrac{1}{E_3} - \dfrac{v_{23}}{E_3}\right)\dot{\sigma}_3 \end{pmatrix} \tag{30}$$

Therefore, the three coefficients E_3, v_{23} and v_{13} cannot be completely identified by only two equations

$$\begin{cases} E_3 = -\dfrac{2\dot{\sigma}_3 v_{13}}{\dot{\varepsilon}_1} & = \dfrac{\dot{\sigma}_3}{\dot{\varepsilon}_3}(1 - v_{23}) \\ v_{23} = -\dfrac{\dot{\varepsilon}_3 E_3}{\dot{\sigma}_3} + 1 & \end{cases} \tag{31}$$

From these equations, the two tangent Poisson ratios v_{23} and v_{13} are related by

$$\frac{-2v_{13}}{1 - v_{23}} = \frac{\dot{\varepsilon}_1}{\dot{\varepsilon}_3} \tag{32}$$

Concretely, the other six coefficients $E_3^+, v_{23}^+, v_{13}^+$ and $E_3^-, v_{23}^-, v_{13}^-$ cannot be identified with an increment of compression stress and an increment of extension stress of direction 3. The radial compression $(0, \dot{\sigma}_3^+)$ and the radial extension $(0, \dot{\sigma}_3^-)$ tests are not the elementary tests, but these two particular stress increment directions $\alpha_{\dot{\sigma}} = 0^\circ$ and $\alpha_{\dot{\sigma}} = 180^\circ$ give two other responses $(\dot{\varepsilon}_1^+, \dot{\varepsilon}_3^+)$ in compression and $(\dot{\varepsilon}_1^-, \dot{\varepsilon}_3^-)$ in extension on the strain envelope. An increment of compression

stress and an increment of extension stress of direction 3 give

$$\begin{cases} E_3^+ = -\dfrac{2\dot{\sigma}_3^+ v_{13}^+}{\dot{\varepsilon}_1^+} \\ v_{23}^+ = -\dfrac{\dot{\varepsilon}_3^+ E_3^+}{\dot{\sigma}_3^+} + 1 \end{cases} \quad \text{and} \quad \begin{cases} E_3^- = -\dfrac{2\dot{\sigma}_3^- v_{13}^-}{\dot{\varepsilon}_1^-} \\ v_{23}^- = -\dfrac{\dot{\varepsilon}_3^- E_3^-}{\dot{\sigma}_3^-} + 1 \end{cases} \tag{33}$$

The two tangent Poisson ratios v_{23}^+ and v_{13}^+ in compression and the two tangent Poisson ratios v_{23}^- and v_{13}^- in extension are related by

$$\frac{-2v_{13}^+}{1-v_{23}^+} = \frac{\dot{\varepsilon}_1^+}{\dot{\varepsilon}_3^+} \quad \text{and} \quad \frac{-2v_{13}^-}{1-v_{23}^-} = \frac{\dot{\varepsilon}_1^-}{\dot{\varepsilon}_3^-} \tag{34}$$

The strain responses of any other stress increment do not permit to assess the three coefficients E_3, v_{23} and v_{13}. Therefore, the constitutive matrices can not be completely determined, even when restricted to the triaxial plane. The first column of the constitutive matrices is identified, but an additional hypothesis is needed to estimate the coefficients of the second column. Nevertheless, we can find the constitutive coefficients with an optimization technique by minimizing the sum of the Euclidian distances between the theoretical and the experimental points of the strain envelopes, and imposing a physical meaning to all the constitutive coefficients: $E^{\pm} > 0$, and $0 < v^{\pm} < 1$. Darve's non-linear interpolation is chosen to estimate the constitutive coefficients. This technique can give several constitutive matrices, but only one set is chosen for the rest of this paper, which means that *the stress history is fixed*.

The tangent Young moduli E (in MPa) and the tangent Poisson ratios v of the constitutive matrices are given directly in a simplified matrix M

$$M = \begin{pmatrix} E_1 & -v_{12} & -v_{13} \\ -v_{21} & E_2 & -v_{23} \\ -v_{31} & -v_{32} & E_3 \end{pmatrix} \tag{35}$$

The first series of probe test at the initial isotropic point $\sigma_1 = 100$ kPa, $\sigma_3 = 100$ kPa, gives the following coefficients of the constitutive matrices:

$$M^+ = \begin{pmatrix} 63{\cdot}86 & -0{\cdot}125 & -0{\cdot}125 \\ -0{\cdot}125 & 16{\cdot}45 & -0{\cdot}832 \\ -0{\cdot}125 & -0{\cdot}832 & 16{\cdot}45 \end{pmatrix}, \qquad M^- = \begin{pmatrix} 34{\cdot}70 & -0{\cdot}330 & -0{\cdot}330 \\ -0{\cdot}330 & 16{\cdot}99 & -0{\cdot}575 \\ -0{\cdot}330 & -0{\cdot}575 & 16{\cdot}99 \end{pmatrix} \tag{36}$$

Note that the two matrices are not identical, indicating an anisotropic internal fabric state of the sample at an isotropic stress state. The Young modulus in extension is nearly half of that in compression. The intermediate stress state at point $\sigma_1 = 200$ kPa, $\sigma_3 = 100$ kPa has the following constitutive matrices:

$$M^+ = \begin{pmatrix} 21{\cdot}57 & -0{\cdot}019 & -0{\cdot}019 \\ -0{\cdot}285 & 32{\cdot}53 & -0{\cdot}900 \\ -0{\cdot}285 & -0{\cdot}900 & 32{\cdot}53 \end{pmatrix}, \qquad M^- = \begin{pmatrix} 151{\cdot}84 & -0.400 & -0.400 \\ -0{\cdot}189 & 20{\cdot}50 & -0.500 \\ -0{\cdot}189 & -0{\cdot}500 & 20{\cdot}50 \end{pmatrix} \tag{37}$$

And the third point at $\sigma_1 = 400\,\text{kPa}$, $\sigma_3 = 100\,\text{kPa}$, gives

$$M^+ = \begin{pmatrix} 4{\cdot}07 & -0{\cdot}001 & -0{\cdot}001 \\ -0{\cdot}572 & 200{\cdot}0 & -0{\cdot}995 \\ -0{\cdot}572 & -0{\cdot}995 & 200{\cdot}0 \end{pmatrix}, \qquad M^- = \begin{pmatrix} 166{\cdot}13 & -0{\cdot}471 & -0{\cdot}471 \\ -0{\cdot}229 & 2{\cdot}00 & -0{\cdot}400 \\ -0{\cdot}229 & -0{\cdot}400 & 2{\cdot}00 \end{pmatrix} \tag{38}$$

Now, we shall compare the predictions of the previous ten restricted models with experimental results.

4.2. *Comparison of interpolation functions*

As noted before, the minimization technique described above does not allow us to obtain the exact solution for each interpolation function. One possible solution is chosen in order to compare different interpolation functions. It appears that the optimized values obtained separately for each interpolation function are close to the solution chosen.

Three aspects are taken into consideration when comparing different interpolation functions, when the values of constitutive matrices are fixed

- The ability to simulate the experimental strain response envelope, with fixed stress history.
- The loss of one-to-one property between the stress increment and the strain increment when restricted to the triaxial plane. The generalization of this aspect to the three-dimensional space is proposed in the next section.
- The continuity of class $\mathscr{C}^1$ of the incremental strain response.

The last two aspects are recommended to obtain a numerical solution of boundary value problems.

The simulated results are plotted two by two in Figures 6–8 to avoid clumsy presentations, the first interpolation function with a continuous line, the second with a dashed line. Four reference points are also indicated by small straight markers. The vertical and thick markers show the two calibrated points at 90° and 270° (axial compression and axial extension stress increments). The horizontal and thin markers indicates the two additional points at 0° and 180° (radial compression and radial extension stress increments). All interpolation functions must pass through the same calibrated points, but the location of the two additional points may vary.

4.2.1. Isotropic stress state: point A. The strain response envelope, in Figure 6, of the isotropic stress state is well simulated by all studied interpolation functions, except for the second interpolation function L4 of Chambon, which has a sharp point at 90° and a near sharp point at 270°, but the $\mathscr{C}^1$-continuity condition is satisfied with this interpolation function. All other response envelopes are convex, and uniqueness is never get lost.

The 10 directions of stress increments are not enough to ensure the $\mathscr{C}^1$-continuity of the experimental strain response envelope. The limited experimental data merely suggest this feature. Nevertheless, with some additional hypotheses concerning the effects of the stress history, the drained circular stress paths corroborated this finding.[21]

The results of the two interpolation functions L9 and L10 of Royis are nearly identical to each other. Therefore, only one result is plotted. This remark applies for the two interpolation functions L5 and L6 of Di Benedetto.

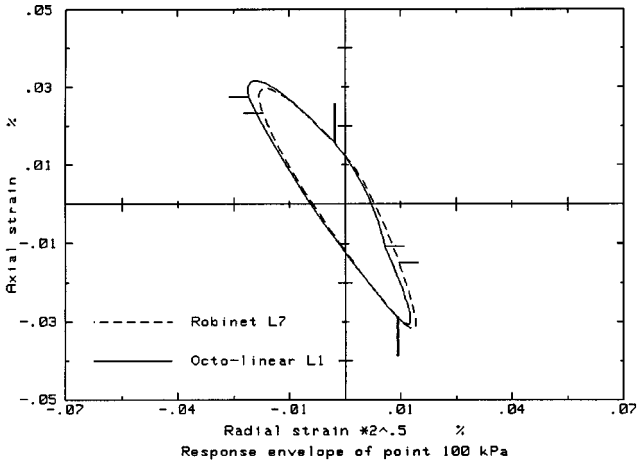

Figure 6a. Strain response envelope of Robinet and octo-linear models at point 100, 100 kPa

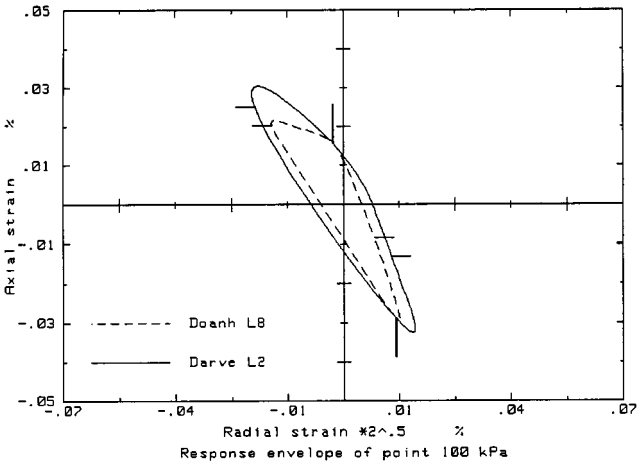

Figure 6b. Strain response envelope of Darve and Doanh models at point 100, 100 kPa

4.2.2. Anisotropic intermediate stress state: point B. Uniqueness is never lost for all simulated strain response envelopes of the anisotropic stress state, Figure 7. The elongated and shifted experimental response envelope can cause some additional problems for the interpolations functions L7 of Robinet, L4 of Chambon and L5 of Di Benedetto. The Chambon second interpolation function has the same sharp point. The fact also appears in the result of Robinet.

The shape of the response envelope is correctly simulated only by the octolinear interpolation function L1 of Darve. The lack of experimental data between 125° and 135° suggests an apex of the response envelope between these two points. This suggestion is confirmed by some simulated response envelopes.

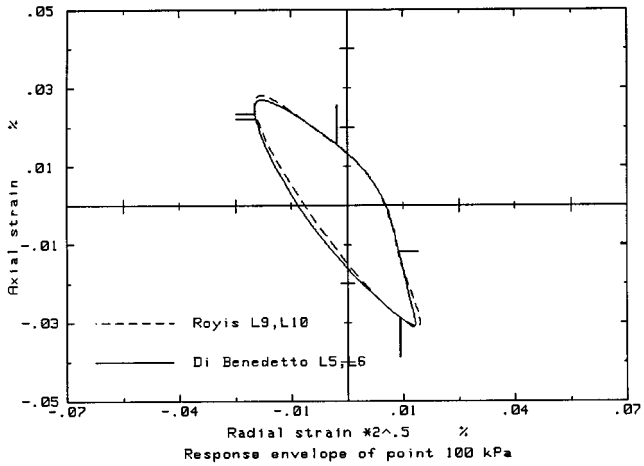

Figure 6c. Strain response envelope of Royis and Di Benedetto models at point 100, 100 kPa

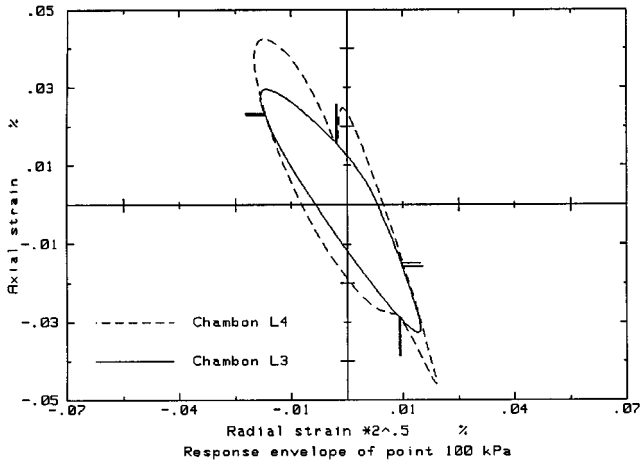

Figure 6d. Strain response envelope of Chambon models at point 100, 100 kPa

4.2.3. Near-failure stress state: point C. The last experimental response envelope degenerates to a flat ellipse. This salient feature cannot be simulated by the eliminated interpolation functions above. The results of Di Benedetto's models L5 & L6 are reduced to a small arc, and uniqueness is lost. The simulation of Darve's non-linear model L2 has a flat response envelope with a long tail in the bottom right quarter, Figure 8.

Note that the main direction of the response envelope as suggested by experimental data is given by the strain response corresponding to the stress increment of 180°. But, a slightly different main direction given by the strain response to the stress increment of 125° is obtained with the octolinear and the non-linear interpolation functions of Darve. This theoretical main direction corresponds to the undrained incremental strain direction.

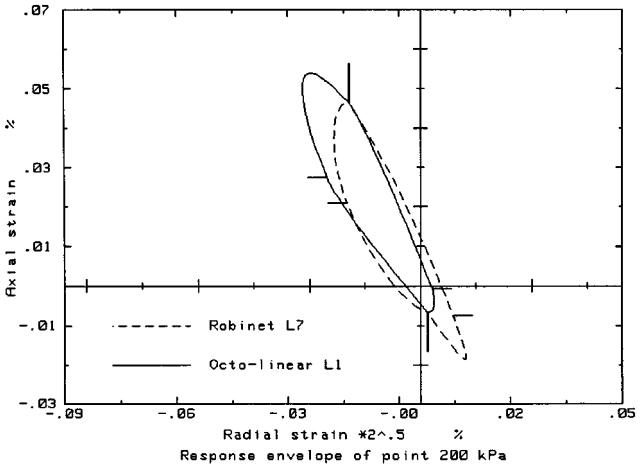

Figure 7a. Strain response envelope of Robinet and octo-linear models at point 200, 100 kPa

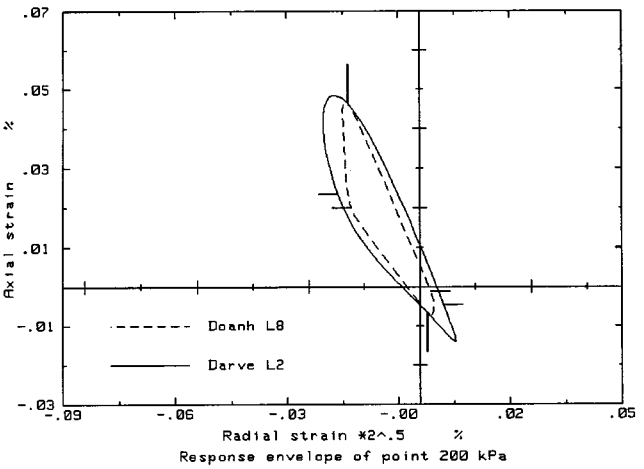

Figure 7b. Strain response envelope of Darve and Doanh models at point 200, 100 kPa

Globally, the strain response envelope at an isotropic stress state is well simulated, but discrepancies between the experimental data and the numerical results increase along with the increasing anisotropic stress state. The Darve octolinear model L1 is the best to simulate the three strain response envelopes; and the non-linear models L3 & L4 of Chambon and L5 & L6 of Di Benedetto fall far behind the experimental data.

4.3. Jacobian of interpolation functions

The strain response envelope, when restricted to the triaxial plane, is a convenient and rapid tool to test any interpolation function of incremental non-linear model. However, it is not self-sufficient to reject the validity of the proposed model.

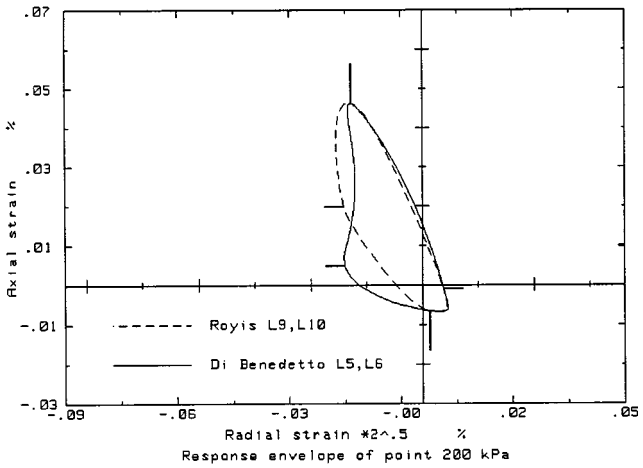

Figure 7c. Strain response envelope of Royis and Di Benedetto models at point 200, 100 kPa

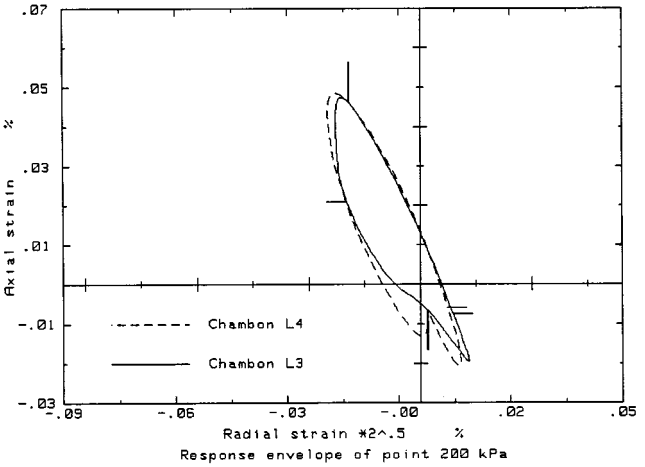

Figure 7d. Strain response envelope of Chambon models at point 200, 100 kPa

The above technique can be generalized three-dimensionally by reconsidering the generalized triaxial paths defined in Section 3.2. For those paths the stress envelope is not a circle of a particular plane, but the unit sphere of $\mathbb{R}^3$. When the stress increment describes this sphere, we can study the variations of the sign of the Jacobian $J = \det(\mathbf{J})$, using a cartographical representation introduced by Royis.[20] Indeed, these variations can be linked (Royis[12]) to the one-to-one property of the constitutive equations $\mathbf{D} = \mathbf{F}(\hat{\boldsymbol{\sigma}})$ since $\mathbf{F}$ is positively homogeneous of degree one in $\hat{\boldsymbol{\sigma}}$ (that property of homogeneity is essential, in a general way there is no link between the one-to-one property of a given function $\mathbf{f}: \mathbb{R}^3 \to \mathbb{R}^3$ of class $\mathscr{C}^1$ and the sign of its Jacobian). For instance, if J is non-zero and keeps the same sign on the unit sphere then $\mathbf{F}$ is one to one. On the

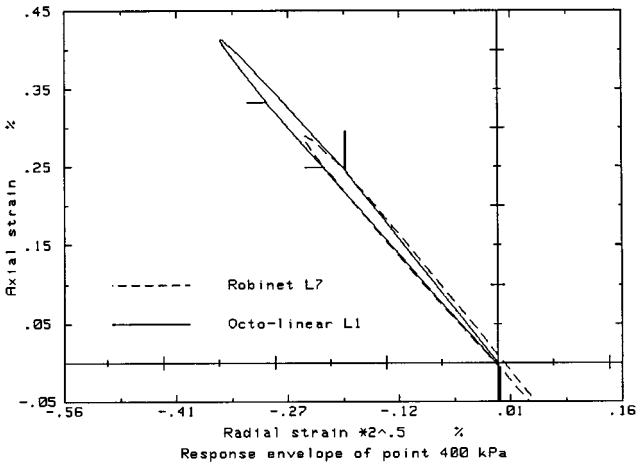

Figure 8a. Strain response envelope of Robinet and octo-linear models at point 400, 100 kPa

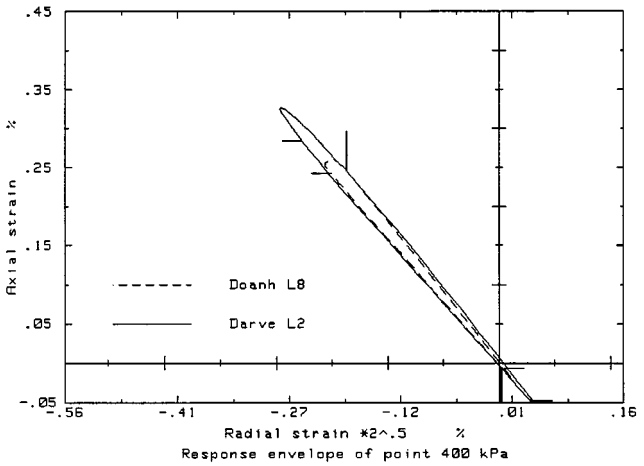

Figure 8b. Strain response envelope of Darve and Doanh models at point 400, 100 kPa

other hand, if there exists two measurable subsets of that unit sphere on which the sign of J is different, then $\mathbf{F}$ is not one to one. For the generalized triaxial paths considered, the direction $\mathbf{d}$ to $\hat{\boldsymbol{\sigma}}$ describes the unit sphere of $\mathbb{R}^3$, so that its components can be expressed by using the spherical co-ordinates θ and φ, as follows:

$$\begin{cases} d_1 = \sin\varphi \\ d_2 = \cos\theta\cos\varphi \quad \text{with} \quad \theta \in \left[-\dfrac{\Pi}{4}, \dfrac{7\Pi}{4}\right] \quad \text{and} \quad \varphi \in \left[-\dfrac{\Pi}{2}, \dfrac{\Pi}{2}\right] \\ d_3 = \sin\theta\cos\varphi \end{cases} \tag{39}$$

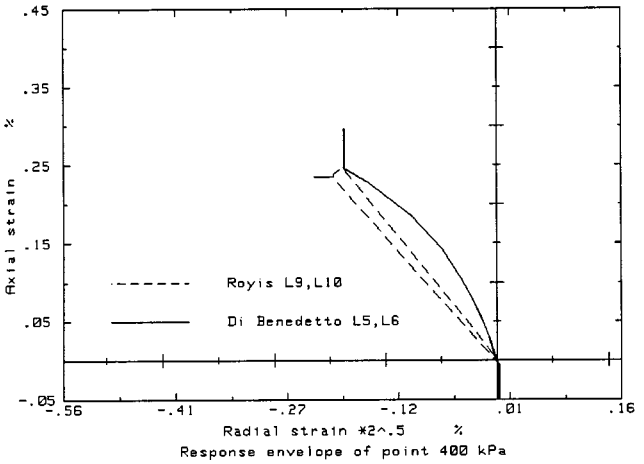

Figure 8c. Strain response envelope of Royis and Di Benedetto models at point 400, 100 kPa

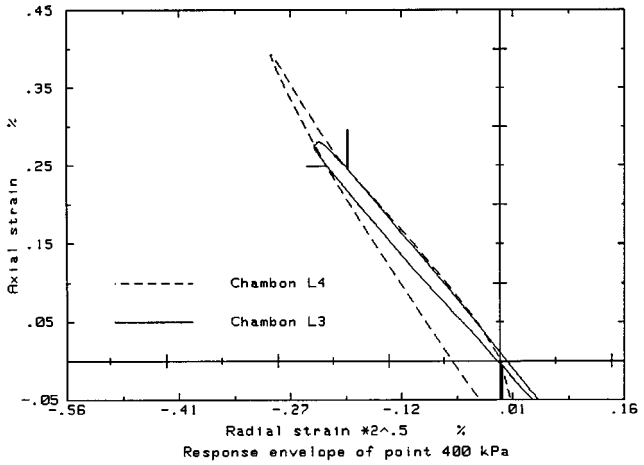

Figure 8d. Strain response envelope of Chambon models at point 400, 100 kPa

The areas of this sphere for which $J > 0$ (resp. $J < 0$) are shown in white (resp. in black). The black zones in this representation indicate the loss of the one-to-one property of the model considered. We selected the highest anisotropic stress state, at $\sigma_1 = 400$ kPa and $\sigma_3 = 100$ kPa. The values of the constitutive matrices are given experimentally by equation (38). Figures 9(a)–9(g) visualize the loss of one-to-one property of seven interpolation functions. Uniqueness is ensured for only three following interpolation functions: the octolinear L1 of Darve and our non-linear models L9 and L10. The completely white figures corresponding to these models are not included here. Table V gives the conclusions of our study based on three requirements.

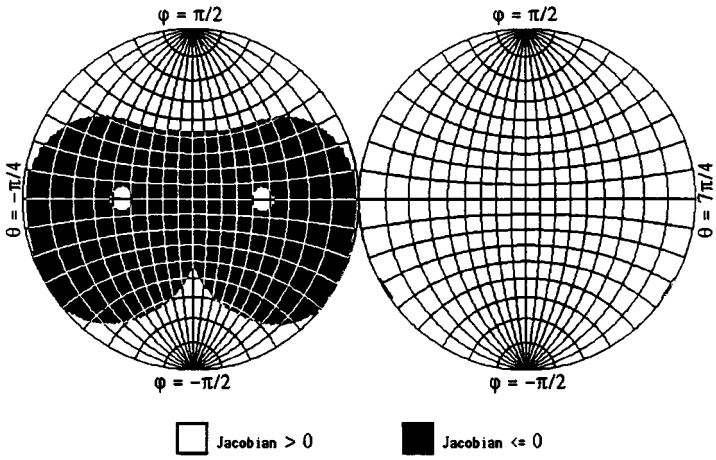

Figure 9a. Sign of the Jacobian for Darve's non linear model

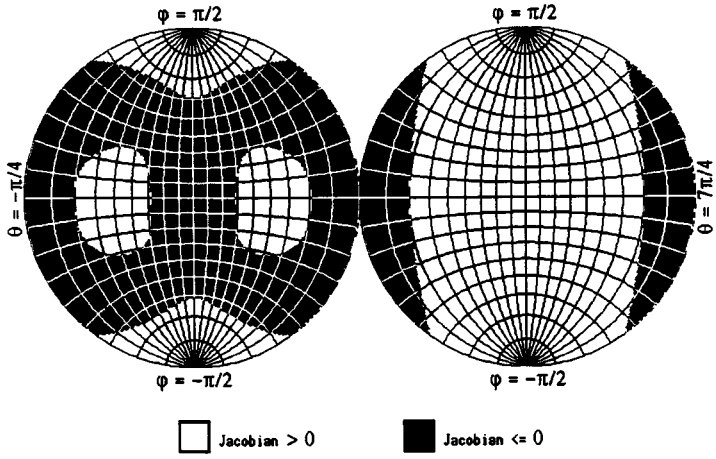

Figure 9b. Sign of the Jacobian for Doanh's non linear model

5. A NEW FAMILY OF INCREMENTALLY NON-LINEAR CONSTITUTIVE MODELS

5.1. Statement of the problem

The comparisons made in the previous Section 4.2 between experimental results and the predictions of the ten restricted models described in Section 3 have shown that none of them meets the triple requirement consisting of $\mathscr{C}^1$-continuity, one-to-one property, and consistency with experience.

The octolinear model L1 shows good agreement with experience and remains one to one, but it is not of class $\mathscr{C}^1$. L9 and L10 are one to one and of class $\mathscr{C}^1$, but their agreement with experience

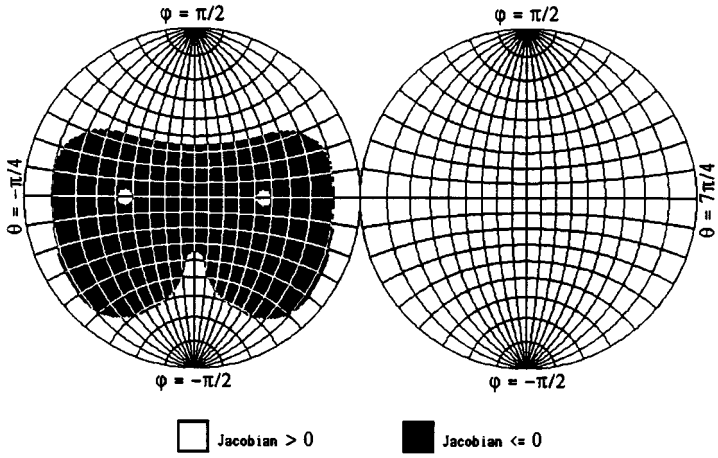

Figure 9c. Sign of the Jacobian for Chambon's model

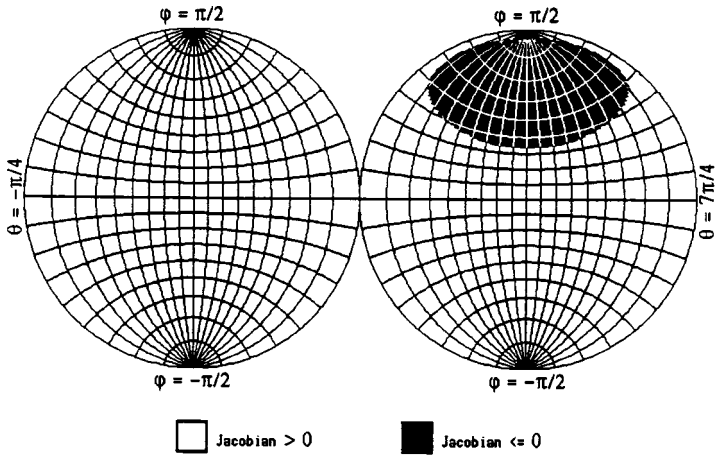

Figure 9d. Sign of the Jacobian for Chambon's non linear model

is not as good as L1's. Finally, L2, L3, L4, L5, L6, L7 and L8 are $\mathscr{C}^1$-continuous, but they are not one to one and show bad agreement with experience. So we intend, in this section, to carry out a new study of interpolation functions of L9 and L10, in order to obtain a better agreement with experimental results.

5.2. Building of the new interpolation functions

Let us consider, for $(i, j) \in \{1, 2, 3\}^2$, the functions r_{ij} that occur in relation (14) when evaluating the components D_i of $\mathbf{D}$, and which are defined by $r_{ij}(d_j) = R_{ij}^{+}\varphi^{+}(d_j) + R_{ij}^{-}\varphi^{-}(d_j) + R_{ij}^{0}\varphi^{0}(d_j)$, with $d_j \in [-1, 1]$ and without any summation on j . For convenience's sake, we shall write these

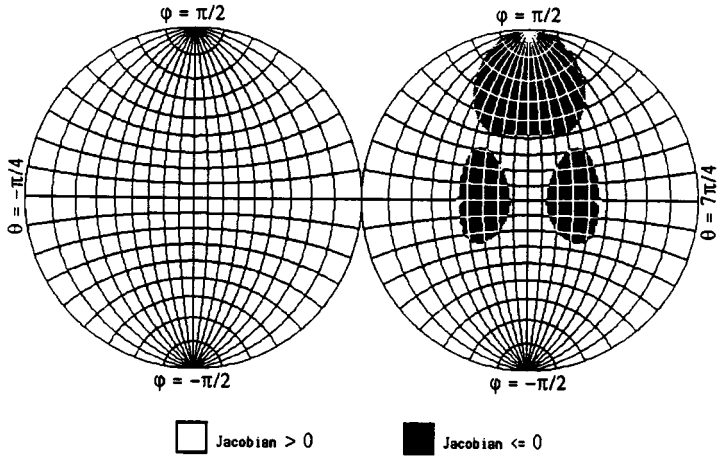

Figure 9e. Sign of the Jacobian for Di Benedetto's first model

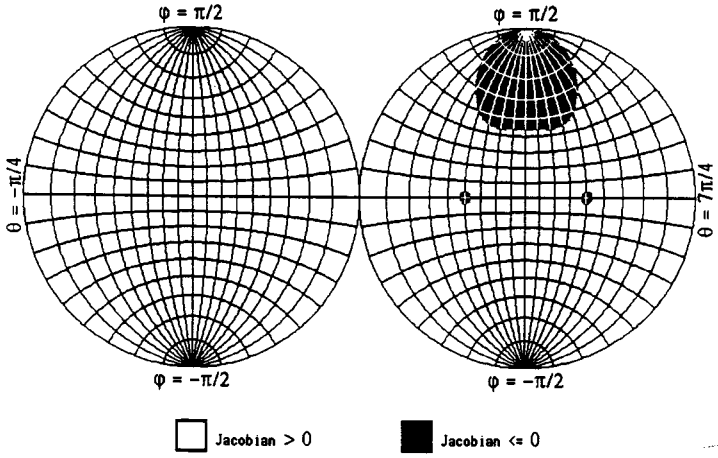

Figure 9f. Sign of the Jacobian for Di Benedetto's second model

functions without mentioning indices i and j, as follows:

$$r(d) = R^{+}\varphi^{+}(d) + R^{-}\varphi^{-}(d) + R^{0}\varphi^{0}(d) \tag{40}$$

The functions $d \to r(d)$, which are linear over each of the intervals $[-1, 0]$ and $[0, 1]$ for the octolinear model L1 and which consist in polynomials of degree 2 as concerns L9 and L10, satisfy the three following conditions:

$$\begin{cases} r(-1) = R^{-} \\ r(0) = 0 \\ r(+1) = R^{+} \end{cases} \tag{41}$$

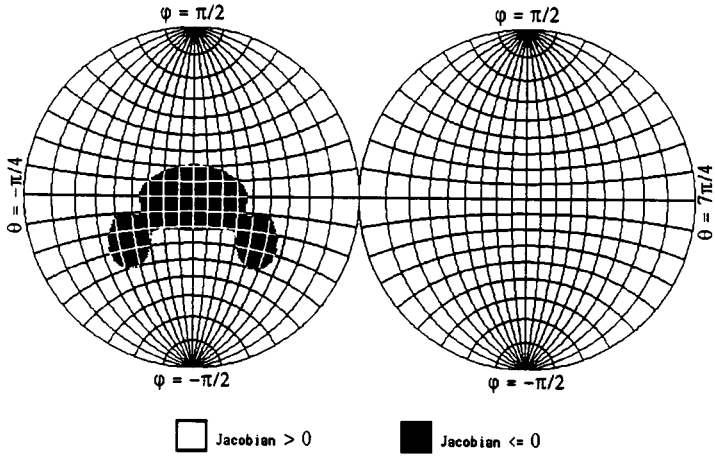

Figure 9g. Sign of the Jacobian for Robinet's non linear model

Table V. Comparison of different interpolation functions

Requirements	L1	L2	L3 & L4	L5 & L6	L7	L8	L9 & L10
Uniqueness	×						×
$\mathscr{C}^1$-continuity		×	×	×	×	×	×
Experimental agreement	×						

Let us then consider the functions $d \to r(d)$ taking the form

$$\begin{cases} r(d) = Ad + B|d|^{1+\alpha} & \text{if } d \in [-1, 0] \\ r(d) = Ad + C|d|^{1+\alpha} & \text{if } d \in [0, 1] \end{cases} \quad \text{with } \alpha \in]0, 1] \tag{42}$$

where A, B and C are three constants to be determined. These functions, which lead to the interpolation functions of L9 and L10 if $\alpha = 1$[20] and which tend to the L1 ones when $\alpha \to 0$, are of class $\mathscr{C}^1$ on $]-1, 1[$ since $\alpha > 0$, and satisfy the second of the conditions (41). So it remains to verify two conditions, which is not enough to determine the three constants A, B and C. On the other hand, in order to avoid any loss of the one-to-one properties of the constitutive equations[17] we have to make, for any given strictly positive value of the ratio $k = -R^-/R^+$, the functions $d \to r(d)$ monotonous. A necessary and sufficient condition, taking account of the definition (42) and of the first and the third of conditions (41), is that the derivative values $r'(-1)$, $r'(0)$ and $r'(+1)$ have all an R^+ sign, which is the same as $-R^-$. That condition, which is obviously necessary, becomes also sufficient since the second derivative values $r''(d)$ keep a constant sign in $]-1, 0[$, as well as in $]0, 1[$. This is why we shall set the three additional conditions

$$\begin{cases} r'(-1) = -K^-R^- & \text{with } K^- > 0 \\ \dfrac{r'(0)}{R^+} > 0 & \\ r'(+1) = K^+R^+ & \text{with } K^+ > 0 \end{cases} \tag{43}$$

These three conditions together with the first and third conditions (41) can be written, taking account of the definition (42)

$$\begin{cases} A - B = -R^- \\ A + C = R^+ \\ A - (1+\alpha)B = -K^- R^- \\ A + (1+\alpha)C = K^+ R^+ \\ \dfrac{A}{R^+} > 0 \\ \text{with } K^+ > 0 \quad \text{and} \quad K^- > 0 \end{cases} \tag{44}$$

This amounts to

$$\begin{cases} A = R^+ \left(\dfrac{1+\alpha-K^+}{\alpha}\right) = -R^- \left(\dfrac{1+\alpha-K^-}{\alpha}\right) \\ B = R^- + A \\ C = R^+ - A \\ \dfrac{A}{R^+} > 0 \\ \text{with } K^+ > 0 \quad \text{and} \quad K^- > 0 \end{cases} \tag{45}$$

or, since $k = -R^-/R^+$ is strictly positive, to

$$\begin{cases} A = R^+ \left(\dfrac{1+\alpha-K^+}{\alpha}\right) = kR^+ \left(\dfrac{1+\alpha-K^-}{\alpha}\right) \\ B = R^- + A \\ C = R^+ - A \\ \text{with } K^+ \in]0, 1+\alpha[\quad \text{and} \quad K^- \in]0, 1+\alpha[\end{cases} \tag{46}$$

So we obtain, after elimination of K^-, the following equivalent system:

$$\begin{cases} A = R^+ \left(\dfrac{1+\alpha-K^+}{\alpha}\right) \\ B = R^- + A \\ C = R^+ - A \\ \text{with } K^+ \in]\max\{0, (1+\alpha)(1-k)\}, 1+\alpha[\end{cases} \tag{47}$$

These relations together with the definition (42) lead to a family of functions $d \to r(d)$ depending on parameter K^+, which are monotonous for any strictly positive value of the ratio $k = -R^-/R^+$

and which met then the requirements set forth at the beginning. However, the variations of these functions with $d \in [-1, 1]$ will be more regular if we let the second derivative values $r''(d)$ keep the same constant sign in both intervals $]-1, 0[$ and $]0, 1[$. Considering definition (42), this amounts to imposing the following additional condition:

$$BC \geqslant 0 \tag{48}$$

which involves, taking relations (47) into account, that K^+ verifies the following inequality:

$$(K^+ - 1)(K^+ - 1 - \alpha + \alpha k) \leqslant 0 \tag{49}$$

The relations in (47) can now be replaced by the following ones:

$$\begin{cases} A = R^+ \left(\dfrac{1 + \alpha - K^+}{\alpha}\right) \\ B = R^- + A \\ C = R^+ - A \\ K^+ \in [K^m, K^M] \\ \text{with } \begin{cases} K^m = \max\{0,(1 + \alpha)(1 - k),\ \min\{1, 1 + \alpha - \alpha\mathrm{k}\}\} \\ K^M = \max\{1, 1 + \alpha - \alpha k\} \end{cases} \end{cases} \tag{50}$$

The relations in equations (42) and (50) define, for any given R^+ and R^- and for any given $\alpha \in]0, 1]$, a family of functions $d \to r(d)$ depending on the parameter K^+. Note that if $k = 1$ then K^+ is necessarily worth 1. In that case we have $A = R^+ = -R^-$, and the unique function $d \to r(d)$ defined by these relations is linear and coincides with that relative to the octolinear model L1. So the considerations developed in this subsection allow us to state the following property.

Property 2. *The functions $d \to r(d)$ defined by relations* (42) *and* (50) *are monotonous for any given strictly positive value of the ratio $k = -R^-/R^+$.*

Now, by setting $R^0 = A$, we can show that the functions $d \to r(d)$ given by the definition (42) and the above relations (50) take the same form as in equation (40), which is the form of the functions $d \to r(d)$ coming from the restricted models L9 and L10 described in Section 3. The new interpolations functions φ^+, φ^- and φ^0 are then as follows:

$$\begin{cases} \varphi^+(d) = d \left(\dfrac{|d| + d}{2}\right)^\alpha \\ \varphi^-(d) = -d \left(\dfrac{|d| - d}{2}\right)^\alpha \quad \text{with } \alpha \in]0, 1] \\ \varphi^0(d) = d(1 - |d|^\alpha) \end{cases} \tag{51}$$

and the component R_{ij}^0 of the new matrices $\mathbf{R}^0$ are obtained, for every $(i,j) \in \{1,2,3\}^2$, from the parameters A defined by the relations (50),

$$\begin{cases} \forall (i,j) \in \{1,2,3\}^2 \text{ and without any summation on } i \text{ and } j: \\ R_{ij}^0 = \left(\dfrac{1+\alpha-K_{ij}^+}{\alpha} \right) R_{ij}^+ \\ \text{with} \begin{cases} K_{ij}^+ \in [K_{ij}^m, K_{ij}^M] \\ K_{ij}^m = \max \left\{ 0, (1+\alpha)\left(1+\dfrac{R_{ij}^-}{R_{ij}^+}\right), \min\left(1, 1+\alpha+\alpha\dfrac{R_{ij}^-}{R_{ij}^+}\right)\right\} \\ K_{ij}^M = \max \left\{ 1, 1+\alpha+\alpha\dfrac{R_{ij}^-}{R_{ij}^+}\right\} \end{cases} \end{cases} \tag{52}$$

The previous relations (51) and (52) together with expressions (14) and (17) define, for given $\mathbf{R}^+$ and $\mathbf{R}^-$ and for any given $\alpha \in]0,1]$, a new family of restricted models depending on the nine parameters K_{ij}^+, $(i,j) \in \{1,2,3\}^2$. As shown previously, if $R_{ij}^- = -R_{ij}^+$ then K_{ij}^+ is necessarily worth 1, which involves $R_{ij}^0 = R_{ij}^+ \ \forall \alpha \in]0,1]$. In particular if $\mathbf{R}^- = -\mathbf{R}^+$ then $\mathbf{R}^0 = \mathbf{R}^+$ $\forall \alpha \in]0,1]$ and the previous family of restricted models is reduced to only one linear model.

The first family of models developed in previous works,[20] from which the restricted models L9 and L10 described in Section 3 come, is obtained by setting $\alpha = 1$ in expressions (51) and (52). Moreover, the following property holds.

Property 3. The restricted models of the family defined by the relations in equations (14), (17), (51) *and* (52) *tend to the octolinear model* L1 *as* α *tends to* 0.

Proof. Clearly it suffices to show that the interpolation functions defined by relations (51) tend to the L1 ones as α tends to 0

$$\begin{cases} \lim\limits_{\alpha \to 0} \varphi^-(d) = \lim\limits_{\alpha \to 0} \left[-d \left(\dfrac{|d|-d}{2} \right)^\alpha \right] = \dfrac{|d|-d}{2} \\ \lim\limits_{\alpha \to 0} \varphi^0(d) = \lim\limits_{\alpha \to 0} \left[d(1-|d|^\alpha) \right] = 0 \\ \lim\limits_{\alpha \to 0} \varphi^+(d) = \lim\limits_{\alpha \to 0} \left[d \left(\dfrac{|d|+d}{2} \right)^\alpha \right] = \dfrac{|d|+d}{2} \end{cases} \tag{53}$$

Now, we shall focus on the new expressions of the restricted models L9 and L10, which will be denoted in the following by L9α and L10α, respectively. □

5.3. *The new restricted models L9α and L10α*

The new family of restricted models developed in the previous Section 5.2 is entirely defined by the relations (51) and (52) together with expressions (14) and (17). The new restricted models L9α

and L10α are then obtained from this family by considering two particular matrices $\mathbf{R}^0$ from the set of matrices given by definition (52). These matrices will be determined in the same way[20] as those given by relations (15) and (16) relating to L9 and L10.

More precisely, the matrix $\mathbf{R}^0$ relating to L9α is obtained by adding to relations (46) the following additional condition binding the strictly positive parameters K^+ and K^-:

$$K^+K^- = 1 \tag{54}$$

Parameter K^+ is then given by the following equation:

$$\begin{cases} (K^+)^2 + (1+\alpha)(k-1)K^+ - k = 0 \\ \text{with } k = -R^-/R^+ > 0 \end{cases} \tag{55}$$

the only strictly positive solution of which is

$$K^+ = \frac{(1+\alpha)(1-k) + \sqrt{((1+\alpha)(1-k))^2 + 4k}}{2} \tag{56}$$

So there remains for us to make sure that K^+ belongs to $[K^m, K^M]$, where K^m and K^M are defined by relations (50).

We shall put, in the following, $a = \sqrt{((1+\alpha)(1-k)^2 + 4k}$. First, note that $a > (1+\alpha)\,|1-k|$ $\forall k > 0$, which involves $K^+ > \max\{0, (1+\alpha)(1-k)\}$. So it only remains for us to show that $K^+ \in [\min\{1, 1+\alpha-\alpha k\}, \max\{1, 1+\alpha-\alpha k\}]$. Let us denote by (P) this property. We have

$$\begin{aligned}
(\mathrm{P}) &\Leftrightarrow (K^+ - 1)(K^+ - 1 - \alpha + \alpha k) \leqslant 0 \\
&\Leftrightarrow (-1 + \alpha - k - \alpha k + a)(-1 - \alpha - k + \alpha k + a) \leqslant 0 \\
&\Leftrightarrow (a - 1 - k)^2 \leqslant \alpha^2 (1-k)^2 \\
&\Leftrightarrow a^2 + (1+k)^2 - 2a(1+k) \leqslant \alpha^2 (1-k)^2 \\
&\Leftrightarrow (1+k)^2 + \alpha(1-k)^2 \leqslant (1+k)a \\
&\Leftrightarrow (1+k)^4 + \alpha^2(1-k)^4 + 2\alpha(1-k^2)^2 \leqslant (1+k)^2 a^2 \\
&\Leftrightarrow -4k\alpha^2(1-k)^2 \leqslant 0
\end{aligned}$$

Therefore, property (P) holds and $K^+ \in [K^m, K^M]$. The components R^0_{ij} of the matrix $\mathbf{R}^0$ relating to L9α are then obtained, for every $(i,j) \in \{1,2,3\}^2$, from relations (52) and (56) after replacing k by $-R^-/R^+$.

$$\begin{cases} \forall (i,j) \in \{1,2,3\}^2 \text{ and without any summation on } i \text{ and } j \\ R^0_{ij} = \dfrac{1+\alpha}{2\alpha}\left(R^+_{ij} - R^-_{ij} - \varepsilon \sqrt{(R^+_{ij})^2 + (R^-_{ij})^2 + 2\,\dfrac{\alpha^2+2\alpha-1}{\alpha^2+2\alpha+1}\,R^+_{ij}R^-_{ij}}\right) \\ \text{with } \varepsilon = +1 \text{ if } R^+_{ij} > 0 \text{ and } \varepsilon = -1 \text{ if } R^+_{ij} < 0 \end{cases} \tag{57}$$

As to the restricted model L10α, it is obtained by adding to relations (46) the following additional condition binding K^+ and K^-:

$$K^+ + K^- = 2 \tag{58}$$

The parameter K^+ must then verify the following equality:

$$1 + \alpha - K^+ = k(-1 + \alpha + K^+) \quad \text{with } k = -R^-/R^+ > 0 \tag{59}$$

which gives

$$K^+ = 1 + \alpha \frac{1-k}{1+k} \tag{60}$$

As for L9α we have now to make sure that $K^+ \in [K^m, K^M]$. To begin with, note that $(1-k)/(1+k) > -1 \ \forall k > 0$. This implies, since $\alpha \in]0, 1]$, that $K^+ > 0$. On the other hand, it follows from (60) that

$$K^+ - (1+\alpha)(1-k) = \frac{(1-\alpha)k + (1+\alpha)k^2}{1+k} > 0 \tag{61}$$

Thus, we have $K^+ > \max\{0, (1+\alpha)(1-k)\}$. So we only have to make sure that $K^+ \in [\min\{1, 1+\alpha-\alpha k\}, \max\{1, 1+\alpha-\alpha k\}]$. But we have, if (P) denotes this last property,

$$\begin{aligned} (\mathrm{P}) &\Leftrightarrow (K^+ - 1)(K^+ - 1 - \alpha + \alpha k) \leqslant 0 \\ &\Leftrightarrow (\alpha - \alpha k)(-\alpha k + \alpha k^2) \leqslant 0 \\ &\Leftrightarrow -k\alpha^2(1-k)^2 \leqslant 0 \end{aligned}$$

Thus, property (P) holds and $K^+ \in [K^m, K^M]$. As for L9α, the components R^0_{ij} of the matrix $\mathbf{R}^0$ relating to L10α are then obtained, for every $(i,j) \in \{1,2,3\}^2$, from relations (52) and (60) after replacing k by $-R^-/R^+$.

$$\begin{cases} \forall (i,j) \in \{1,2,3\}^2 \text{ and without any summation on } i \text{ and } j \\ R^0_{ij} = 2\, \dfrac{R^+_{ij} R^-_{ij}}{R^-_{ij} - R^+_{ij}} \end{cases} \tag{62}$$

Note that this matrix is the same as that of L10 given by equation (16) and does not depend on parameter α, unlike that of L9α.

Finally, let us point out that the gradient tensor $\mathbf{J}$ of the restricted model L9α and L10α, and more generally of all restricted models developed in this section, is given by the relations (22) and (23) obtained in Section 3.3 for L1, L2, L3, L7, L8, L9 and L10, with the following expressions for the derivatives $\varphi^{+\prime}$, $\varphi^{-\prime}$ and $\varphi^{0\prime}$ of the interpolation functions:

$$\begin{cases} \varphi^{+\prime}(d) = (1+\alpha)\, \left(\dfrac{|d|+d}{2}\right)^{\alpha} \\ \varphi^{-\prime}(d) = -(1+\alpha)\, \left(\dfrac{|d|-d}{2}\right)^{\alpha} \\ \varphi^{0\prime}(d) = 1 - (1+\alpha)\, |d|^{\alpha} \end{cases} \tag{63}$$

5.4. *Comparison with experimental strain response envelope*

The new parameter α cannot be determined directly by the strain response envelope in the triaxial plane. Nevertheless, a value 0·01 within its range]0, 1] can be selected to simulate the experimental data. Figures 10–12 show the comparison with the three experimental response envelopes when $\alpha = 0{\cdot}01$. This small value of α ensures a good agreement with the experimental data, since the new interpolation function tends to the octolinear model. This interpolation function meets the three requirements.

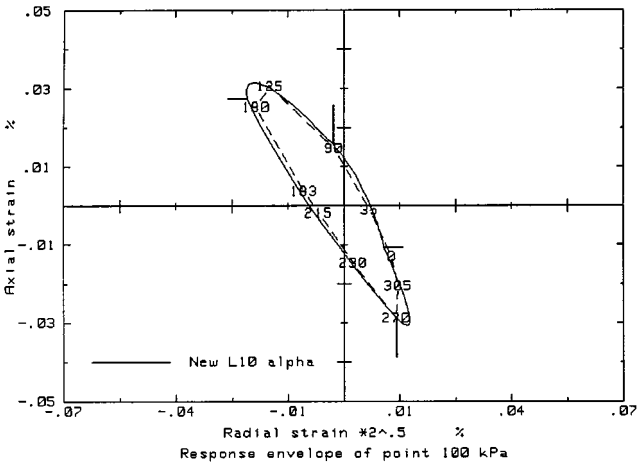

Figure 10. Comparison of new interpolation function at point 100, 100 kPa

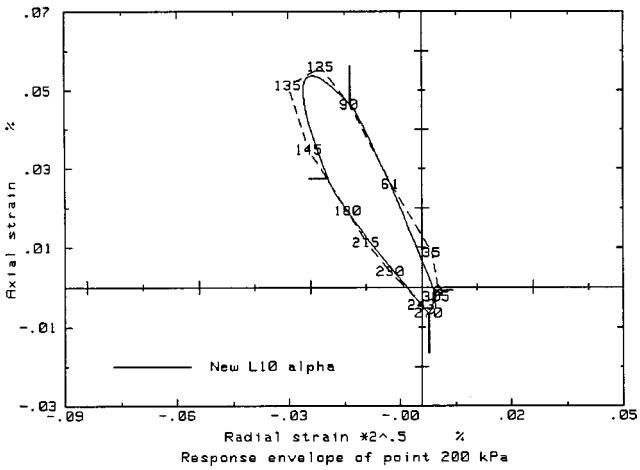

Figure 11. Comparison of new interpolation function at point 200, 100 kPa

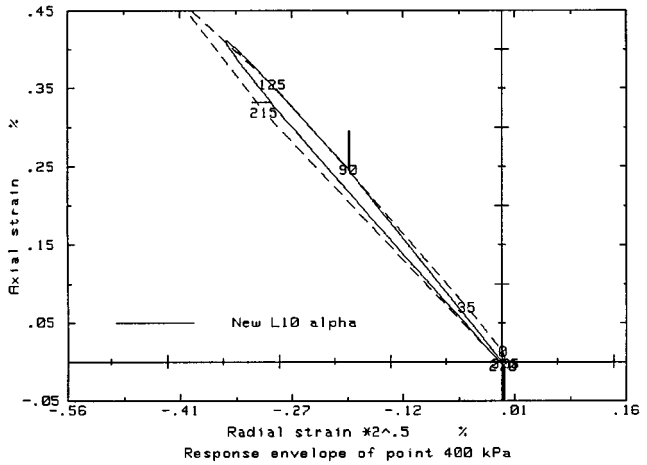

Figure 12. Comparison of new interpolation function at point 400, 100 kPa

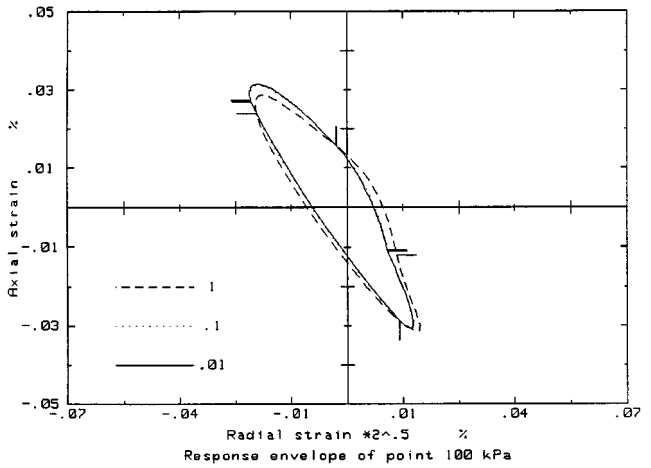

Figure 13. Effect of alpha parameter on the new interpolation function, (at point 100, 100 kPa)

The effects of parameter α on the shape of the strain response envelope are presented in Figures 13–15. The incremental continuity is not affected.

Other research groups at the LGM laboratory are working to enhance the strain response envelope with initial non-axisymmetric stress states including principal stress rotation, and thereby gain a deeper understanding of the soil behaviour. New experimental data will provide the opportunities to check the correct behaviour of the new interpolation functions.

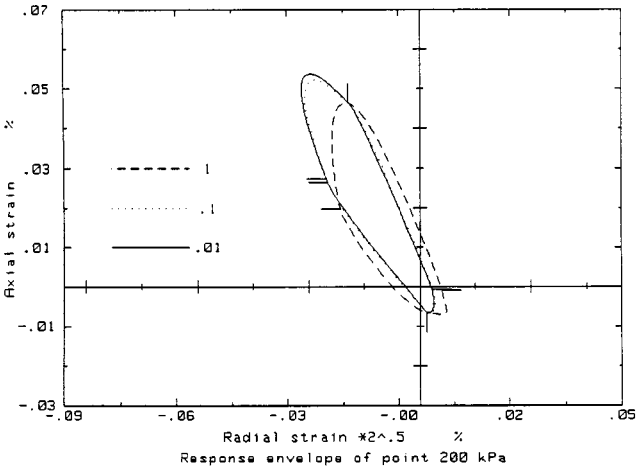

Figure 14. Effect of alpha parameter on the new interpolation function, (at point 200, 100 kPa)

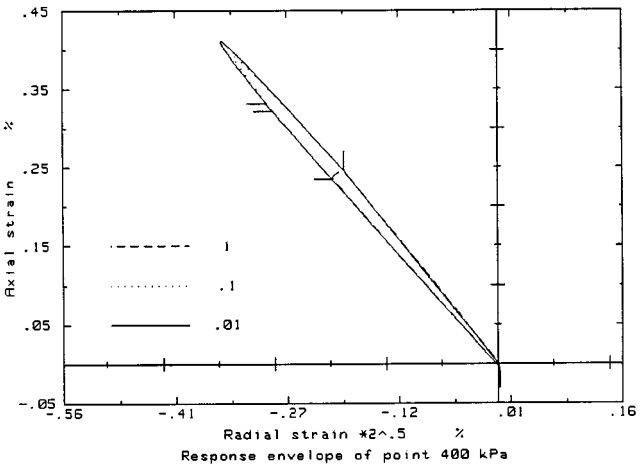

Figure 15. Effect of alpha parameter on the new interpolation function, (at point 400, 100 kPa)

6. CONCLUSIONS

Different interpolation functions involved in the incrementally non-linear constitutive equations are reviewed in this paper, using the strain response envelopes based on experimental results. The general property of uniqueness is also checked with a cartographical technique. A new family of interpolation functions is introduced. This family meets the three requirements set forth at the beginning of this paper: $\mathscr{C}^1$-continuity of strain response envelope, correct description of the experimental data, and respect of the one-to-one property.

NOTATIONS

$\boldsymbol{\sigma}$	Cauchy stress tensor
$\boldsymbol{\epsilon}$	linearized tensor of small strains
σ_1, σ_3	axial and radial principal stresses for triaxial test
$\varepsilon_1, \varepsilon_3$	axial and radial principal strains for triaxial test
$\sigma_1 - \sigma_3$	deviatoric stress
R	failure ratio
$\alpha_{\delta\sigma}$	direction of the stress increment in the plane $(\sigma_1, \sqrt{2}\sigma_3)$
$\alpha_{\delta\varepsilon}$	direction of the strain increment in the plane $(\varepsilon_1, \sqrt{2}\varepsilon_3)$
$\mathbf{D}$	strain rate tensor
$\mathbf{W}$	spin tensor
$\dot{\boldsymbol{\sigma}}, \dot{\boldsymbol{\epsilon}}$	time derivatives of $\boldsymbol{\sigma}$ and $\boldsymbol{\epsilon}$
$\hat{\boldsymbol{\sigma}}$	Jaumann derivative of $\boldsymbol{\sigma}$
$\mathbf{T}$	a given second-order symmetric tensor on $\mathbb{R}^3$
$\mathbf{T}$	the vector of $\mathbb{R}^6$ isometrically associated with $\mathbf{T}$
$\mathbf{F}$	constitutive tensorial function
$\mathbf{F}$	six-dimensional constitutive function associated with $\mathbf{F}$
$\mathbf{J}$	second-order gradient tensor of $\mathbf{F}$
λ	a multiplicative scalar parameter
$\mathbf{d}, \|\hat{\boldsymbol{\sigma}}\|$	direction and Euclidian norm of $\hat{\boldsymbol{\sigma}}$
$\mathbf{R}^+, \mathbf{R}^-$	tangent constitutive matrices
$E_i^+, E_i^-, i \in \{1, 2, 3\}$	tangent Young moduli
$v_{ij}^+, v_{ij}^-, (i, j) \in \{1, 2, 3\}^2$	tangent Poisson ratios
$\mathbf{R}^0$	constitutive matrice function of $\mathbf{R}^+$ and $\mathbf{R}^-$
$\boldsymbol{\psi}^+, \boldsymbol{\psi}^-, \boldsymbol{\psi}^0$	interpolation vectors
$\varphi^+, \varphi^-, \varphi^0$	interpolation functions
$N_i^+, N_i^-, i \in \{1, 2, 3\}$	scalar functions of $\mathbf{R}^+$ and $\mathbf{R}^-$
ϕ	scalar function of $\mathbf{R}^+$, $\mathbf{R}^-$ and $\mathbf{d}$
$\mathbf{M}$	constitutive matrice
$\mathbf{J}^+, \mathbf{J}^-, \mathbf{J}^0$	gradient tensors of $\|\hat{\boldsymbol{\sigma}}\|\boldsymbol{\psi}^+$, $\|\hat{\boldsymbol{\sigma}}\|\boldsymbol{\psi}^-$ and $\|\hat{\boldsymbol{\sigma}}\|\boldsymbol{\psi}^0$
$(\dot{\varepsilon}_1, \dot{\varepsilon}_3)$	strain axisymmetric triaxial response
$(\dot{\varepsilon}_1^+, \dot{\varepsilon}_3^+)$	strain axisymmetric triaxial response in compression
$(\dot{\varepsilon}_1^-, \dot{\varepsilon}_3^-)$	strain axisymmetric triaxial response in extension
M, M^+, M^-	simplified constitutive matrices
θ, φ	spherical co-ordinates
$r_{ij}, (i, j) \in \{1, 2, 3\}^2$	scalar functions of $\mathbf{R}^+, \mathbf{R}^-$ and $\mathbf{d}$
r	the function r_{ij} for a given $(i, j) \in \{1, 2, 3\}^2$
R^+, R^-	the components of $\mathbf{R}^+$ and $\mathbf{R}^-$ for a given $(i, j) \in \{1, 2, 3\}^2$
k	ratio $-R^-/R^+$
α, K^+, K^-	scalar parameters of the function r
K^m, K^M	scalar functions of α and k
$K_{ij}^+, (i, j) \in \{1, 2, 3\}^2$	scalar parameter of the component R_{ij}^0 of $\mathbf{R}^0$
$K_{ij}^m, K_{ij}^M, (i, j) \in \{1, 2, 3\}^2$	scalar function of α, R_{ij}^+ and R_{ij}^-

REFERENCES

1. J. C. Robinet, M. Mohkam, T. Doanh and M. Deffayet, 'A non linear constitutive law for soils', in G. Gudehus and F. Darve (eds.), *Constitutive Relations for Soils*, A. A. Balkema, 1982, pp. 405–418.
2. T. Doanh, H. Di Benedetto, G. Golcheh and K. Kharchafi, 'Non linear incremental constitutive equation: Application to sands', in A. Saada and G. Bianchini (eds), *Constitutive Equations for Granular Non Cohesive Soils*, A. A. Balkema, 1989, pp. 255–276.
3. F. Darve and S. Labanieh, 'Incremental constitutive laws for sand and clays. Simulation of monotonic and cyclic tests', *Int. J. Num. Anal. Meth. Geomech.* **6,** 243–275 (1982).
4. G. Gudehus, 'A comparison of some constitutive laws for soils under radially symmetric loading and unloading', in *Proc. 3rd Numer. Meth. in Geomechanics*, Vol. 4, A. A. Balkema, 1979, 1309–1323.
5. G. Gudehus and D. Kolymbas, 'Numerical testing of constitutive relations for soils', in *Proc. 5th Numer. Meth. in Geomechanics*, Vol. 1, A. A. Balkema, 1985, pp. 63–81.
6. W. Wu and D. Kolymbas, 'Numerical testing of the stability criterion for hypoplastic constitutive equations', *Mech. Mater.*, **9,** 245–253 (1990).
7. T. Doanh and P. Royis, 'A comparative study of incremental non-linear constitutive equations', in *Proc. 7th Int. Conf. on Comput. Meth. and Adv. in Geomech.*, Vol. 2, A. A. Balkema, 1991, pp. 605–610.
8. R. Chambon, J. Desrues, W. Hammad, and R. Charlier, 'CloE, a new rate-type constitutive model for geomaterials Theoretical basis and implementation', *Int. J. Numer. Anal. Meth. Geomech.*, **18,** 253–278 (1994).
9. H. Di Benedetto and F. Darve, 'Comparison de lois rhéologiques en cinématique rotationnelle', *Mécanique Théorique Appl.*, **2,** 769–798 (1983).
10. G. Gudehus, 'Requirements for constitutive relations for soils', in Z. Bazant, (ed.), *Mechanics of Geomaterials*, Wiley, New York, 1985, pp. 47–63.
11. F. Darve, *Geomaterials, Constitutive Equations and Modelling*, Elsevier, Amsterdam, 1990, pp. 213–238.
12. P. Royis, 'Modélisation par éléments finis des Géomatériaux', *Thèse d'Habilitation à Diriger des Recherches* (*spécialité Mécanique et Energétique*), Institut National Polytechnique de Grenoble, Mars 1995.
13. M. Boulon and A. Alachaher, 'A new incrementally non linear constitutive law for finite element application in geomechanics', *Comput. Geotech.*, **17,** 177–201 (1995).
14. W. Wu and E. Bauer, 'A simple hypoplastic constitutive model for sand', *Int. J. Numer. Anal. Meth. in Geomech.*, **18,** 833–862 (1994).
15. D. Kolymbas, I. Herle and P. A. von Wolffersdorff, 'Hypoplastic constitutive equation with internal variables', *Int. J. Numer. Anal. Meth. in Geomech.*, **19,** 415–446 (1995).
16. G. Gudehus, 'A comprehensive constitutive equation for granular materials', *Soils Found.*, **36,** 1–12 (1996).
17. P. Royis, 'Formulation mathématique de lois de comportement—Modélisation numérique de problèmes aux limites en mécanique des solides déformables', *Thèse de Doctorat d'Ingénieur* (*spécialité Mécanique*), Institut National Polytechnique de Grenoble, Juillet 1986.
18. R. Chambon, 'Une loi rhéologique incrémentale non linéaire pour les sols non visqueux', *J. Mécanique Théorique Appl.*, **3,** 521–544 (1984).
19. H. Di Benedetto, 'Modélisation du comportement des géomatériaux—Application aux enrobés et aux bitumes', *Thèse de Doctorat ès Sciences Physiques*, Université Scientifique et Médicale de Grenoble, 1987.
20. P. Royis, 'Interpolations and one-to-one properties of incremental constitutive laws—A family of incrementally nonlinear constitutive laws', *Euro. J. Mech. A/Solids*, **8,** 385–411 (1989).
21. T. Doanh, 'Behaviour of Hostun sand under drained circular stress path', In *Proc. 2nd Numerical Models in Geomechanics*, Jackson, 1986, pp. 205–211.

